Geochemistry Geophysics Geosystems G3
AN ELECTRONIC JOURNAL OF THE EARTH SCIENCES
Published by AGU and the Geochemical Society

Article
Volume 6, Number 6
21 June 2005
Q06008, doi:10.1029/2005GC000938
ISSN: 1525-2027

Subduction-related metasomatism in the thinning lithosphere: Evidence from a composite dunite-orthopyroxenite xenolith entrained in Mesozoic Laiwu high-Mg diorite, North China Craton

Li-Hui Chen

State Key Laboratory of Lithospheric Evolution, Institute of Geology and Geophysics, Chinese Academy of Sciences, Beijing 100029, China

Now at State Key Laboratory for Mineral Deposits Research, Department of Earth Sciences, Nanjing University, Nanjing 210093, China (chenlh@nju.edu.cn)

Xin-Hua Zhou

State Key Laboratory of Lithospheric Evolution, Institute of Geology and Geophysics, Chinese Academy of Sciences, Beijing 100029, China (xhzhou@mail.igcas.ac.cn)

[1] The North China Craton (NCC) lost its Archean keels in the Phanerozoic. Prevalent and intensive magmatism, mineralization, and development of extensional basins in the late Mesozoic NCC imply that the late Mesozoic could be the key stage for this transformation. Ultramafic xenoliths in the Early Cretaceous high-Mg diorites of Shandong province might provide key information about the transformation of subcontinental lithospheric mantle (SCLM) beneath the NCC. Here we present a unique composite dunite-orthopyroxenite xenolith from Tietonggou, one of the high-Mg diorite-dominated plutons in Laiwu, Shandong province. The petrography and mineral chemistry of the xenolith suggest complicated metasomatic processes, which occurred before its entrainment in the host magma. Early stage metasomatism includes the growth of intergranular phlogopite and clinopyroxene and the development of a phlogopite- and amphibole-bearing clinopyroxenite veinlet. Late-stage metasomatism (termed Si (Na) metasomatism) is characterized by the growth of secondary orthopyroxene, Na-rich plagioclase and amphibole with resorption of olivine and clinopyroxene, and the decomposition of phlogopite. The xenolith has exceptionally high concentrations of Na_2O and Al_2O_3 and shows enrichments in Cs, Rb, Th, U, K, and the light rare earth elements. It also shows positive Pb and Sr anomalies and negative Nb, Ta, P, and Ti anomalies in a primitive mantle normalized spider gram. The geochemistry, as well as the elevated $\delta^{18}O$, suggests that this Si (Na) metasomatism is associated with subduction. The secondary orthopyroxene in the orthopyroxenite portion of the xenolith has exceptionally low Mg# values, which may be the result of reaction between silica-rich melts and olivine with high melt:rock ratios. Mg-Fe disequilibrium of the minerals in the orthopyroxenite indicates that Si (Na) metasomatism may have been introduced shortly before entrainment of the xenolith in the host magma. Correlation of the Sr-Nd-Pb isotopic compositions of ultramafic xenoliths, high-Mg diorites, and adakitic granites of the Tietonggou indicates there may be a genetic relationship between these rocks. Thus we propose that the SCLM beneath Shandong may have been metasomatized by a slab-derived melt. Since Si (Na) metasomatism occurred at the key stage of lithospheric thinning, oceanic subduction might have been involved in the thinning process.

Components: 11,290 words, 14 figures, 5 tables.

Keywords: mantle xenolith; mantle metasomatism; lithosphere thinning; subduction; North China Craton.

Index Terms: 1025 Geochemistry: Composition of the mantle; 3621 Mineralogy and Petrology: Mantle processes (1038); 3613 Mineralogy and Petrology: Subduction zone processes (1031, 3060, 8170, 8413).

Received 7 February 2005; **Revised** 11 April 2005; **Accepted** 27 April 2005; **Published** 21 June 2005.

Chen, L.-H., and X.-H. Zhou (2005), Subduction-related metasomatism in the thinning lithosphere: Evidence from a composite dunite-orthopyroxenite xenolith entrained in Mesozoic Laiwu high-Mg diorite, North China Craton, *Geochem. Geophys. Geosyst.*, *6*, Q06008, doi:10.1029/2005GC000938.

1. Introduction

[2] The stability and fate of subcontinental lithospheric mantle (SCLM) is an important unresolved issue. The North China Craton (NCC) is one of the oldest Archean cratons on the earth [*Jahn et al.*, 1987; *Liu et al.*, 1992], and is surrounded by the NE China fold belts, the Qinlin-Dabie-Sulu orogenic belts, and the Yangtze craton (Figure 1). Mantle xenoliths from the Paleozoic kimberlites of Mengyin and Fuxian suggest that the SCLM beneath the NCC is thick (180–200 km), cold and refractory, like other Archean cratons [*Menzies et al.*, 1993; *Griffin et al.*, 1998]. However, mantle xenoliths from the Cenozoic basalts suggest a thin (<80 km), hot and fertile SCLM in the eastern NCC [*Fan et al.*, 2000]. Thus the SCLM beneath the eastern NCC suffered a massive transformation (or thinning) in the Phanerozoic. Recent evidence from Os isotopes of peridotite xenoliths also supports such a conclusion [*Gao et al.*, 2002; *Wu et al.*, 2003]. Although the direct mechanism and geodynamics remain controversial, the prevalent and intensive late Mesozoic magmatism, mineralization, and the development of extensional basins in the region imply that the late Mesozoic could be a key stage for this major lithospheric transformation [*Menzies and Xu*, 1998; *Xu*, 2001; *Zhang et al.*, 2002, 2003; *Zhou et al.*, 2002; *Yang et al.*, 2003; *Zhai et al.*, 2004; *Xu et al.*, 2004b, 2004c; *Xu et al.*, 2004]. The discovery of ultramafic xenoliths in the Cretaceous high-Mg diorites and basalts of the eastern NCC in recent years, such as Laiwu (125–131 Ma), Zibo (112–129 Ma), Fangcheng (125 Ma), Fuxin (100 Ma), and Jiaozhou (74 Ma), not only provide direct SCLM samples of the late Mesozoic [*Xu et al.*, 1993; *Zheng et al.*, 1999; *Zhang et al.*, 2002; *Xu et al.*, 2003a; *Yan et al.*, 2003; *Chen and Zhou*, 2004], but also more crucial information about the thinning process.

[3] Shandong province is located in the central part of the eastern NCC, and is divided into two parts, west Shandong (Luxi area) and east Shandong (Jiaodong area), by the giant Tan-Lu wrench fault (Figure 1). Early Cretaceous igneous rocks are ubiquitous in Shandong province, and include gabbro-dominated plutons in the north of west Shandong [*Dong*, 1987; *Guo et al.*, 2001], high-Mg diorite-dominated plutons in west Shandong [*Dong*, 1987; *Chen*, 2001; *Xu et al.*, 2004], granite-dominated plutons in east Shandong [*Yang and Zhou*, 2001], medium-mafic volcanics or lamprophyres distributed throughout the whole province [*Qiu et al.*, 2002; *Ying*, 2002; *Guo et al.*, 2003; *Yang et al.*, 2004], and a few carbonatites in Laiwu and Zibo [*Ying*, 2002; *Ying et al.*, 2004]. Laiwu basin is situated in the center of west Shandong, near the Tan-Lu fault (Figure 1). There are four high-Mg diorite-dominated plutons in Laiwu, including Kuangshan, Jiaoyu, Jinniushan, and Tietonggou [*Dong*, 1987; *Chen*, 2001]. Abundant ultramafic xenoliths had been found in the Tietonggou intrusion [*Xu et al.*, 1993; *Chen*, 2001; *Chen and Zhou*, 2004]. K-Ar and Ar-Ar dating of the intrusion gives an age of 125–133 Ma [*Chen*, 2001; *Xu et al.*, 2004b], which is consistent with the SHRIMP U-Pb age (130.2 Ma) of the Jiaoyu intrusion [*Xu et al.*, 2004]. The lithology, mineral chemistry, equilibrium temperature (690–790°C), and metasomatic characteristics of the ultramafic xenoliths indicate that they might be derived from the shallow lithosphere (the crust-mantle transitional zone) and were metasomatized by hydrous silica-rich melts [*Chen and Zhou*, 2004]. Similar Sr-Nd isotopic compositions indicate that there may be genetic links between these xenoliths and their host rocks [*Chen and Zhou*, 2004]. Here we report the petrology, geochemistry and Sr-Nd-Pb-O isotopic composition of a unique composite xenolith (dunite + orthopyroxenite), which presents more detailed metasomatic information than previously reported xenoliths. Furthermore, this paper provides evidence on the timing of the metasomatism and the source characteristics of the metasomatic liquids, which may help to understand the thinning process of the SCLM of the NCC.

2. Petrography

[4] Xenolith LW0006, with a size of 6 × 7 × 14 cm, is the most extremely metasomatized sample found so far in the xenolith suite of the Tietonggou

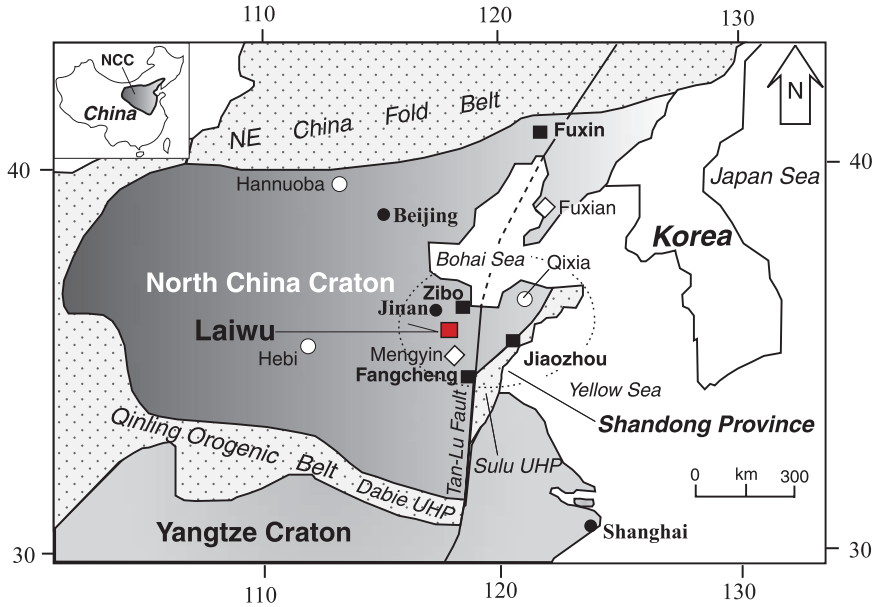

Figure 1. Laiwu and other xenolith localities in the North China Craton (modified from *Zhang et al.* [2002]), with selected Cenozoic basalt-hosted xenolith localities, e.g., Hannuoba and Qixia, shown as open circles, Paleozoic kimberlite-hosted xenolith localities (Mengyin, Fuxian) shown as open diamonds, and Mesozoic diorite/basalt-hosted xenolith localities (Laiwu, Zibo, Jiaozhou, Fuxin, Fangcheng) shown as solid squares. Major cities are shown as solid circles. Shandong province is showed by a dotted circle.

pluton. We prepared a large thin section to view the whole structure of the specimen (Figure 2), and two small thin sections for mineral analysis (Figure 3). The specimen is a composite xenolith, composed mainly of phlogopite-rich orthopyroxenite, and several minor dunite cores (Figure 2). The dunites have heterogeneous abundances of spinel. Some dunite cores are enriched in spinel, up to 30%, such as dunite A in the left thin section of Figure 3, whereas others have low spinel contents, less than 2%, such as dunite B in the right thin section of Figure 3. All dunites exhibit porphyroclastic texture and recrystallization textures. Porphyroblasts of olivine are commonly kinked, while fine-grained recrystallized olivines are free of kink bands. The boundary between the host diorite and the orthopyroxenite portion of the xenolith is sharp (Figures 2 and 4a). A hornblendite selvage is in contact with a dunite core in the xenolith (Figures 2 and 4b). The boundaries between dunite and orthopyroxenite are sharp and curved (Figures 2, 3, and 4c), and the composite xenolith resembles a conglomerate with dunite pebbles (Figure 2).

[5] Dunite A is characterized by a high abundance of spinel (Figure 3). The spinel is usually euhedral or subhedral in shape and 50–400 μm in size. One composite veinlet found in dunite A is composed primary of orthopyroxenite with minor clinopyroxenite (Figure 5a). The clinopyroxenite occurs

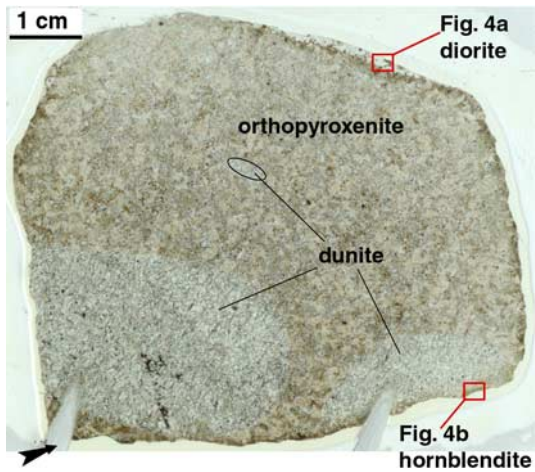

Figure 2. Whole thin-section view of xenolith LW0006 (scanning picture). Three gravel-like dunite portions are enclosed by orthopyroxenite in this thin section. White minerals are olivine, dark minerals are spinel, yellowish minerals are porphyroblasts of orthopyroxene, and yellow minerals are phlogopite. The boundaries between dunite and orthopyroxenite are sharp. The arrow points to mechanical damage. Relict of host diorite and the hornblendite selvage can be seen in the open red squares, which are shown in Figure 4a and Figure 4b, respectively.

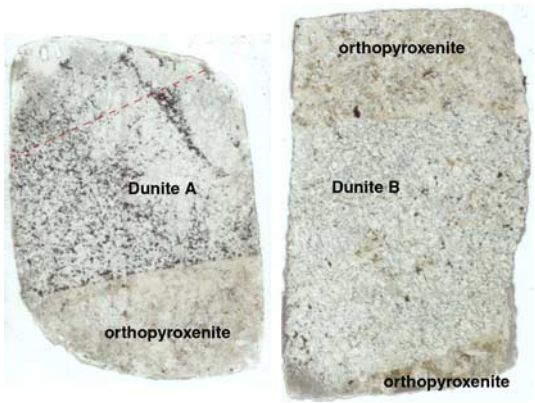

Figure 3. Scanning pictures of the two thin sections of xenolith LW0006. Two different dunites can be seen in these thin sections. Dunite A (left) is characterized by an enrichment of dark spinel, whereas dunite B (right) is characterized by low abundances of spinel. A veinlet found in dunite A is shown by the red dotted line. Disseminated yellow phlogopite can be seen in dunite B.

only at the center of the veinlet, which has a turbid appearance due to exsolution of the minerals (Figure 5a). The clinopyroxenite is composed of clinopyroxene, phlogopite, and amphibole (Figure 5b), whereas the orthopyroxenite consists only of orthopyroxene with a clean appearance.

[6] Dunite B has a low abundance of spinel (Figure 3). The spinel is anhedral and small (less than 50 μm). Anhedral phlogopites are disseminated unevenly between olivines (Figure 6a). A back-scattered electron (BSE) image shows that the minerals located interstitial to the olivines include not only phlogopite, but also clinopyroxene, orthopyroxene, plagioclase, and amphibole (Figure 6b). Clinopyroxene and phlogopite are partly replaced by orthopyroxene, plagioclase and amphibole, but the relationship between clinopyroxene and phlogopite is unclear. Orthopyroxene is also situated along the boundaries between olivine grains (top left of Figure 6b) and the contacts between orthopyroxene and olivine are straight and sharp.

[7] The orthopyroxenite has complicated mineral compositions and metasomatic textures (Figure 7). Orthopyroxenes and phlogopites are the main phases, with minor olivine, plagioclase and spinel, calcite, zircon, rutile, and apatite as accessory minerals. Porphyroblasts of orthopyroxene have turbid appearances due to the presence of numerous inclusions, such as resorbed olivine, spinel, phlogopite as well as fluid inclusions (Figure 7a). Phlogopite is commonly ragged and decomposes into anhydral orthopyroxene and plagioclase

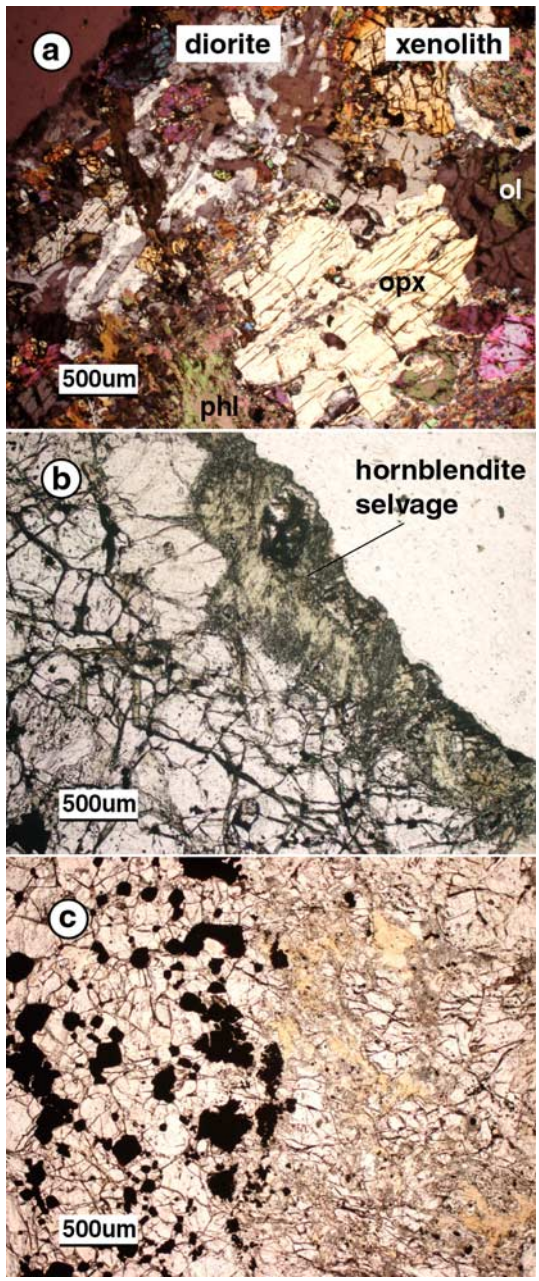

Figure 4. Micrographs of xenolith LW0006. (a) Sharp boundary between host diorite (left) and the orthopyroxenite of the xenolith (right); one coarse orthopyroxene (including several small olivine inclusions) is decomposed into smaller orthopyroxenes along the boundary. Crossed-polarized light. (b) Thin hornblendite selvage at the margin of dunite B. Plane-polarized light. (c) Sharp boundary between dunite A (left) and the phlogopite-rich orthopyroxenite (right). Dark spinels at the boundary are smaller than those in the inner zone of the dunite but are much coarser than those in the orthopyroxenite. Plane-polarized light. Abbreviations: ol, olivine; opx, orthopyroxene; phl, phlogopite.

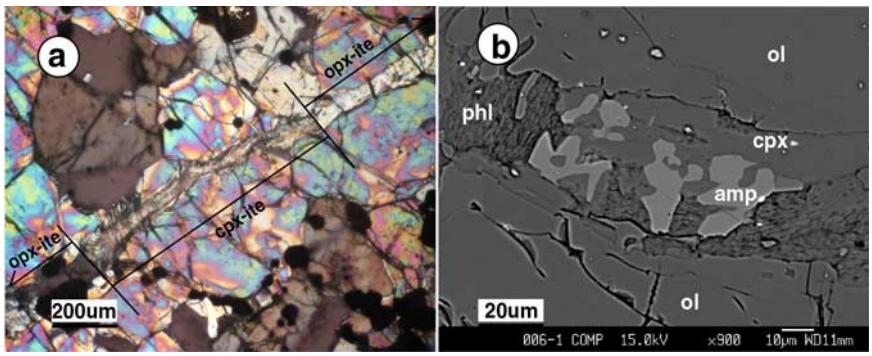

Figure 5. Metasomatic veinlet in dunite A of xenolith LW0006. (a) The veinlet is a composite composed of phlogopite- and amphibole-bearing clinopyroxenite in the center and orthopyroxenite along the two sides. Exsolution texture is observed in the amphiboles associated with the clinopyroxenite. Crossed-polarized light. (b) Back-scattered electron (BSE) image of the clinopyroxenite portion of the composite veinlet. Abbreviations: opx-ite, orthopyroxenite; cpx-ite; clinopyroxenite; ol, olivine; cpx, clinopyroxene; phl, phlogopite; amp, amphibole.

(Figure 7c). Olivines exist as resorbed inclusions in orthopyroxene and phlogopite (Figures 7a and 7b). Fine-grained anhedral spinels (most less than 20 μm size) occur throughout. Some spinels exist as inclusions in orthopyroxene and phlogopite, while others constitute as pseudomorphs of euhedral spinel.

3. Mineral Chemistry

[8] Mineral chemistry was analyzed with a JEOL Superprobe JXA 8100 electron-probe microanalyzer (EPMA) at the School of Earth and Space Sciences, Peking University and a JEOL JXA 8800M EPMA at the Department of Earth Sciences, Nanjing University, using an accelerating voltage of 15 kv, beam currents of 1×10^{-8}A and 2×10^{-8}A respectively, and 1 μm beam size. The counting times for Ni, Mn, and Ca in olivine are longer than that for other elements. Selected microprobe analyses of dunite A, dunite B, and orthopyroxenite are listed in Tables 1–3, respectively.

3.1. Olivine

[9] Olivine in dunite A is chemically heterogeneous. The olivine in spinel-rich portion has the highest Mg# value (Mg# = Mg/(Mg + Fe^{2+}) × 100) of 94.4, while olivine in the spinel-depleted area has a lower Mg# value of 92.3. Olivine in dunite B has a lower Mg# value of 88.2 and olivine in orthopyroxenite has the lowest Mg# values of 85.5–86.6. The range of Mg# values in primitive olivines from other peridotite xenoliths in Tietonggou is from 87 to 93.

3.2. Spinel

[10] Spinel in dunite A is characterized by high Cr_2O_3 (56 wt%), MgO (10.9 wt%), and low total

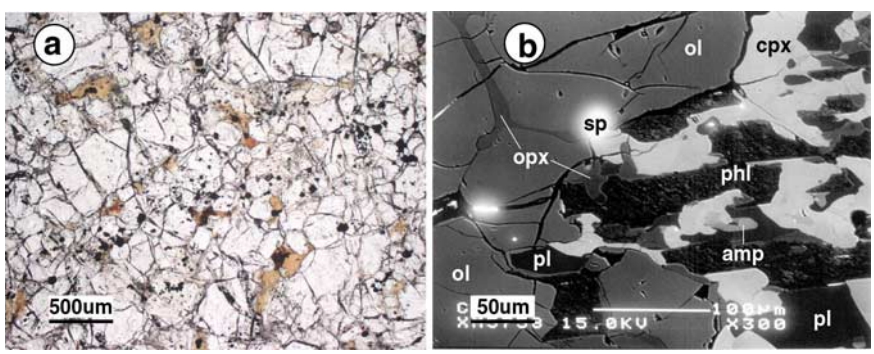

Figure 6. Metasomatic textures in dunite B of xenolith LW0006. (a) Yellow phlogopites, as well as other metasomatic minerals, are disseminated in dunite. Plane-polarized light. (b) BSE image shows five minerals located interstitial to the olivines, including clinopyroxene (cpx), phlogopite (phl), orthopyroxene (opx), Na-rich plagioclase (pl), and Na-rich amphibole (amp). Clinopyroxene are separated by phlogopite, and both clinopyroxene and phlogopite are partly replaced by orthopyroxene, plagioclase, and amphibole. Orthopyroxene also can be seen at the triple junction and along the boundaries of the olivines.

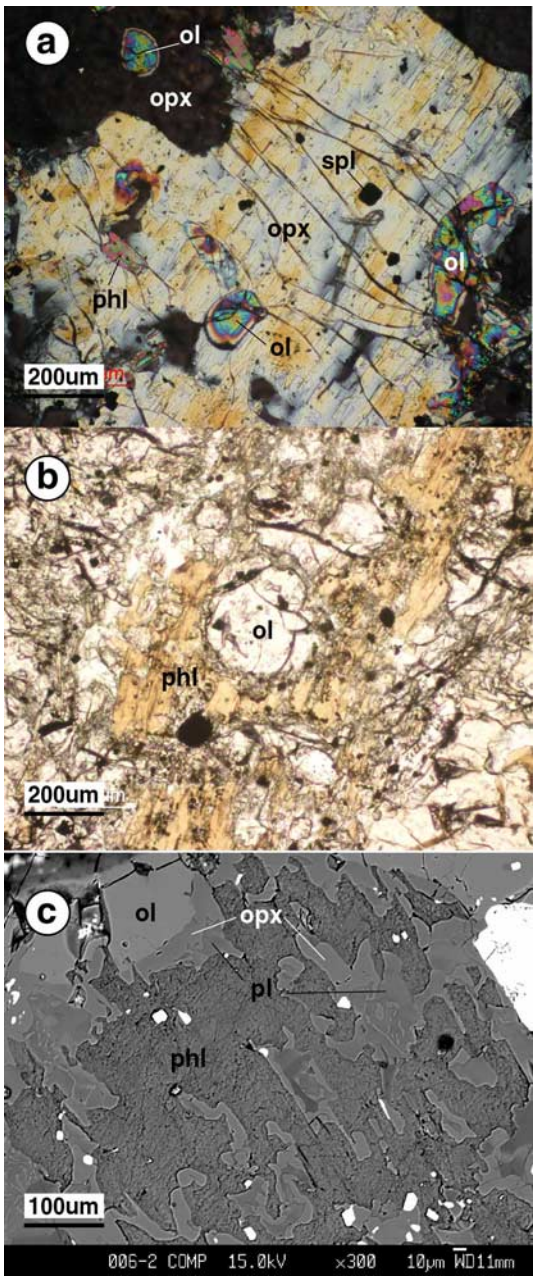

Figure 7. Metasomatic textures in the orthopyroxenite of xenolith LW0006. (a) Porphyroblast of orthopyroxene includes many small mineral inclusions (olivine, phlogopite, and spinel). Crossed-polarized light. (b) Olivine is partly enclosed by a ragged phlogopite. Plane-polarized light. (c) Decomposition texture of coarse phlogopite (phl → opx + pl). BSE image. Abbreviations: ol, olivine; spl, spinel; opx, orthopyroxene; phl, phlogopite; pl, plagioclase.

FeO (20.9 wt%), Al_2O_3 (9.3 wt%), TiO_2 (0.28 wt%) concentrations, with high Mg# (54.9) and Cr# (Cr# = Cr/(Cr + Al + Fe^{3+}) × 100) (80.3). Spinel in dunite B has lower concentrations of Cr_2O_3 (40 wt%), MgO (8.1 wt%), and higher concentrations of total FeO (30.5 wt%), Al_2O_3 (19.6 wt%), and TiO_2 (0.32 wt%) contents, with lower Mg# (34.8) and Cr# (60.6). The Mg# and Cr# of spinel in the orthopyroxenite have broad ranges of 34.8–38 and 46–70, respectively. Spinel rims usually has lower Mg# and Cr# values and higher TiO_2 concentrations than the spinel cores (Table 3). Such chemical heterogeneity is common in spinels from Tietonggou xenoliths.

3.3. Orthopyroxene

[11] Orthopyroxene in the xenolith has low Al_2O_3 contents (0.8–2.6 wt%), which is consistent with orthopyroxene from other Tietonggou xenoliths, but is different from orthopyroxene in mantle xenoliths entrained by Cenozoic basalts of the NCC (Figure 8). The orthopyroxene in this xenolith can be distinguished from the primary orthopyroxene of Tietonggou peridotite xenoliths by the broad range of Cr_2O_3 (0–0.95 wt%) and CaO concentrations (0.31–0.89) (Figure 8). Orthopyroxene in the veinlet of dunite A has the highest Mg# (91.8–92.6) and Cr_2O_3 concentrations (0.42–0.95 wt%), and the lowest concentrations of Al_2O_3 (0.79–1.38 wt%) in the composite xenolith. Orthopyroxene in dunite B has an intermediate Mg# (88.1–88.7), and intermediate concentrations of Cr_2O_3 (0.15–0.60 wt%) and Al_2O_3 (1.20–1.68 wt%). Orthopyroxene in the orthopyroxenite has a broad compositional range with the lowest Mg# (85.2–87.9) and Cr_2O_3 concentrations (0–0.31 wt%), and the highest Al_2O_3 concentrations (1.0–2.6 wt%) in the composite xenolith.

3.4. Phlogopite

[12] Phlogopite in the clinopyroxenite part of the composite veinlet of Dunite A is characterized with high Mg# value (95.7–95.9), high CaO (0.24–1.38 wt%), and low TiO_2 content (0.04–0.08 wt%). Disseminated phlogopite in Dunite B is characterized with low Mg# value (89.2–90.2), low CaO (0–0.20 wt%), and high TiO_2 content (2.3–3.4 wt%). Ragged phlogopite in the orthopyroxenite part is characterized with broad composition and low Mg# value (89.1–92.0), low CaO (0–0.13 wt%), and high TiO_2 contents (1.1–2.2 wt%).

3.5. Clinopyroxene

[13] Clinopyroxene in the clinopyroxenite portion of the composite veinlet of dunite A is Ca-rich diopside with a high Mg# (95.2). The clinopyroxene contains no Cr_2O_3, which is different from the

Table 1. Representative EMP Analyses of Minerals in Dunite A of Xenolith LW0006[a]

Number	1	2	3	4	5	6	7	8
Mineral	ol	ol	spl	opx	opx	cpx	amp	phl
SiO_2	41.55	42.63		57.35	57.15	55.82	52.17	42.29
TiO_2	0.02		0.28	0.02			0.07	0.08
Al_2O_3	0.01		9.26	1.13	1.38	0.79	2.57	14.53
Cr_2O_3	0.06		56.14	0.95	0.52			
FeO	7.60	5.53	20.89	5.12	5.15	1.65	1.68	2.06
MnO	0.04	0.05	0.29	0.03	0.06			
MgO	51.30	52.02	10.93	35.03	34.62	18.39	18.76	25.52
CaO	0.01	0.07		0.41	0.35	23.17	20.46	1.38
NiO	no.	0.58	0.23	no.	no.	0.04	0.13	0.18
Na_2O						0.28	0.36	1.06
K_2O		0.00			0.00	0.12	0.94	7.56
F	0.15	no.	no.	0.06	0.09	no.	no.	no.
Total	100.68	100.89	98.01	100.07	99.28	100.25	97.14	94.67
Mg#	92.3	94.4	54.9	92.4	92.3	95.2	95.2	95.7
			Cr#80.3					

[a] FeO, total iron; ol, olivine; spl, spinel; phl, phlogopite; cpx, clinopyroxene; amp, amphibole; pl, plagioclase; no., not analyzed; Mg# = Mg/(Mg + Fe^{2+}) × 100; Cr# = Cr/(Cr + Al) × 100. 1–3, primary minerals of Dunite A, 4–8, secondary minerals in the composite veinlet; 1, olivine by the veinlet; 2, olivine in the spinel-rich zone.

primitive clinopyroxene (Cr-rich diopside with 0.63–1.22 wt% Cr_2O_3) of other Tietonggou peridotites. Disseminated clinopyroxene in dunite B has lower Mg# (89.6–91.0), high Cr_2O_3 concentrations (0.40–0.84).

3.6. Amphibole

[14] Amphibole in the clinopyroxenite of the composite veinlet of dunite A exhibits high Mg# (95.2), high SiO_2 (52.2 wt%) and CaO (20.5 wt%), and low Al_2O_3 (2.6 wt%), Na_2O (0.36 wt%), TiO_2 (0.07 wt%) and Cr_2O_3 (<0.01 wt%) concentrations. Amphibole in dunite B exhibits low Mg# value (86.3), low concentrations of SiO_2 (44.3 wt%) and CaO (13.1 wt%), and high concentrations of Al_2O_3 (12.1 wt%), Na_2O (2.84 wt%), TiO_2 (1.81 wt%), and Cr_2O_3 (1.1 wt%), which is consistent with Na-rich amphiboles in orthopyroxenite veinlets observed in other Tietonggou xenoliths.

3.7. Plagioclase

[15] Plagioclase in dunite B and in the orthopyroxenite are both enriched in Na_2O (Na_2O = 2.7–7.9 wt%) and show broad compositional ranges ($An_{32-75}Ab_{67-25}$). They have depleted K contents (K_2O < 0.06 wt%), which differ from plagioclase in the host diorite (K_2O = 0.13–0.45 wt%).

4. Analytical Procedures and Results

[16] The specimen was first cut into several pieces. One piece selected from the inner part of the

Table 2. Representative EMP Analyses of Minerals in Dunite B of Xenolith LW0006[a]

Number	1	2	3	4	5	6	7	8	9	10
Mineral	ol	ol	spl	cpx	cpx	opx	opx	phl	amp	pl
SiO_2	40.47	39.61	0.01	53.64	51.33	56.18	55.86	39.61	44.34	54.80
TiO_2			0.32	0.08	0.34	0.08	0.06	2.33	1.81	0.02
Al_2O_3	0.02		19.60	1.69	3.19	1.68	1.40	16.31	12.05	28.60
Cr_2O_3			40.64	0.40	0.83	0.60	0.28	0.83	1.11	
FeO	11.98	11.37	30.46	3.09	3.43	7.98	7.84	4.29	4.77	0.16
MnO	0.09	0.18	0.36	0.13	0.07	0.09	0.02	0.11	0.00	
MgO	47.18	48.74	8.14	17.04	16.62	33.13	33.58	21.59	16.90	0.09
CaO		0.02		23.12	23.03	0.75	0.66		13.12	10.73
Na_2O	0.01			0.50	0.61	0.01	0.00	0.88	2.84	5.65
K_2O			0.03	0.00	0.02	0.01		9.43	0.64	0.04
F	0.13	0.11		0.22	0.13	0.14	0.06	0.31	0.31	0.13
Total	99.82	99.98	99.55	99.82	99.54	100.57	99.74	95.55	97.75	100.16
Mg#	87.5	88.4	39.1	90.8	89.6	88.1	88.4	90.0	86.3	An51.1
			Cr#58.2							Ab48.7

[a] 1–3, primary minerals; 4–10, secondary minerals.

Table 3. Representative EMP Analyses of Minerals in the Orthopyroxenite Part of Xenolith LW0006[a]

Number	1	2	3	4	5	6	7	8	9	10	11
Mineral	ol	spl	spl	spl	opx	opx	opx	phl	phl	pl	pl
SiO_2	39.73		0.10		56.87	57.21	56.00	38.24	39.32	54.97	61.39
TiO_2		1.16	0.27	0.66		0.08	0.11	1.87	1.12		
Al_2O_3		14.98	7.22	12.99	1.03	1.03	2.59	15.96	16.52	29.58	24.45
Cr_2O_3	0.06	34.30	54.53	42.12	0.12	0.23	0.03	1.19	0.90	0.07	
FeO	13.08	40.22	30.09	34.02	8.06	8.82	9.59	4.71	3.52	0.27	
MnO			0.19	0.37		0.13	0.28				
MgO	46.80	7.15	6.92	7.51	32.69	31.89	30.95	21.67	22.61	0.03	0.03
CaO	0.01				0.89	0.84			0.09	9.76	6.84
NiO	0.46	0.17	0.15	0.22	0.09	0.06		0.27	0.17		0.02
Na_2O		0.03			0.06	0.01	0.02	1.02	2.00	5.56	7.85
K_2O					0.01			8.77	6.36	0.06	0.17
ZnO			0.09	0.27							
Total	100.14	98.02	99.57	98.16	99.82	100.29	99.57	93.69	92.60	100.29	100.75
Mg#	86.4	34.8	35.3	37.8	87.9	86.6	85.2	89.1	92.0	An49.1	An32.2
		Cr#60.6	Cr#83.5	Cr#68.5						Ab50.5	Ab66.8

[a] 2 is a fine-grained spinel. 3 and 4 are the core and the rim of a relatively coarse spinel, respectively.

xenolith was mainly composed of orthopyroxenite (>95 vol.%) with minor dunite. This portion was broken into small fragments about 1 ~ 5 mm in size, which were rinsed with distilled water and dried in an oven. The dried fragments were then milled into 200 mesh for chemical analysis. Major elements were measured on glass fusion discs by RIX-2100 X-ray fluorescence at the Key Laboratory for Continental Dynamics, Northwest University (Xi'an, China). The precision (relative 2δ error) for major elements is estimated to be <1%. Results (in wt%) are shown in Table 4.

[17] Analysis of trace elements and isotopic compositions was done at the Institute of Geology and Geophysics, Chinese Academy of Sciences. Chemical processing of the sample was carried out in an ultra-clean laboratory. Trace elements in the xenolith were analyzed by a Finnigan MAT ICP-MS following the procedures outlined by *Jin and Zhu* [2000], together with three standards and a blank. On the basis of the repeated analyses of standards and parallel samples, the 2σ error of the analyses is estimated to be <20% for Co, Cr, Ga, Ba, Zr, Ta, Pb, and <10% for Li, Sc, V, Ni, Cu, Rb, Sr, Y, Nb, Cs, Hf, Th, U, Tm, Lu and <5% for the rare earth elements (REE) except Tm and Lu. Results (in ppm) are shown in Table 4.

[18] Sr-Nd-Pb isotopic analyses were carried out using a VG354 mass spectrometer according to the procedures of *Yang and Zhou* [2001]. During the

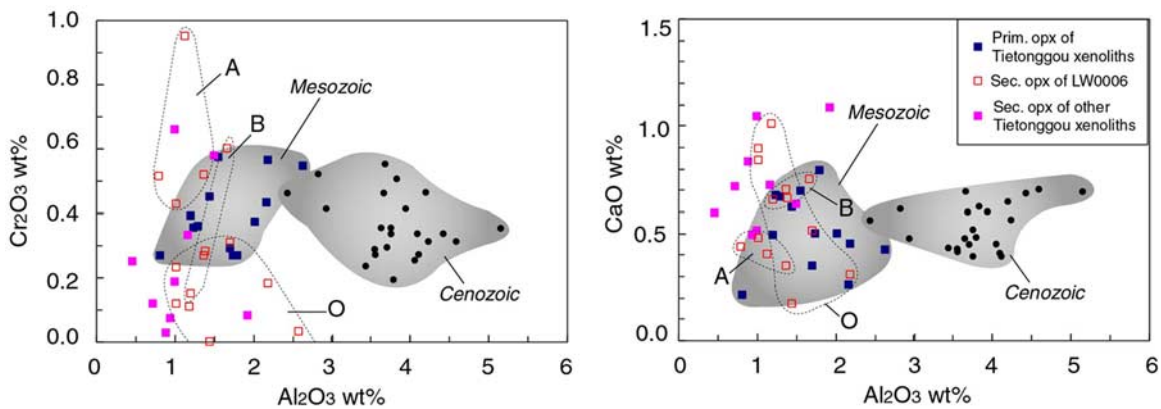

Figure 8. Chemical compositions of orthopyroxene in xenolith LW0006. A, dunite A; B, dunite B; O, orthopyroxenite. Orthopyroxenes in Tietonggou xenoliths have lower Al_2O_3 concentrations than those in Cenozoic peridotite xenoliths [*Rudnick et al.*, 2004]. Cr_2O_3 and CaO concentrations in secondary orthopyroxenes have broader ranges than primitive orthopyroxenes in Tietonggou xenoliths. In xenolith LW0006 the Cr_2O_3 contents of secondary orthopyroxenes in dunite A are higher than those of dunite B and the orthopyroxenite.

Table 4. Major Elements and Trace Elements of Xenolith LW0006[a]

SiO_2	TiO_2	Al_2O_3	$Fe_2O_3{}^T$	MnO	MgO	CaO	Na_2O	K_2O	P_2O_5	LOI	Total
46.01	0.26	5.14	10.58	0.15	34.25	2.17	0.65	0.67	0.08	0.10	100.1
Li	Sc	V	Cr	Co	Ni	Cu	Ga	Rb	Sr	Y	Zr
9.79	4.06	49.6	2711	104	1336	16.3	6.22	19.6	174	4.18	49.3
Nb	Cs	Ba	Hf	Ta	Pb	Th	U	La	Ce	Pr	Nd
2.19	1.39	114	1.22	0.18	89.2	2.68	0.84	9.41	16.5	1.83	6.87
Sm	Eu	Gd	Tb	Dy	Ho	Er	Tm	Yb	Lu		
1.24	0.399	1.19	0.16	0.88	0.17	0.48	0.08	0.49	0.07		

[a] Major element units are oxide wt%, and trace element units are ppm.

period in which the analyses were carried out, the measured $^{87}Sr/^{86}Sr$ value of NBS607 was 1.20055 ± 2, repeat analyses of the liquid standard La Jolla gave $^{143}Nd/^{144}Nd$ values of 0.511855 ± 9, the measured $^{143}Nd/^{144}Nd$ value of BCR1 was 0.512651 (9) and repeat analyses (6×) of NBS981 yielded $^{204}Pb/^{206}Pb$ = 0.05900 ± 8, $^{207}Pb/^{206}Pb$ = 0.91439 ± 17 and $^{208}Pb/^{206}Pb$ = 2.16441 ± 97, respectively. The measured Sr-Nd-Pb isotopic ratios of this sample (>95 vol.% orthopyroxenite and <5 vol.% dunite) are listed in Table 5.

[19] For analyses of $\delta^{18}O$, the sample was first reacted with BrF_5, after which the liberated oxygen was converted to CO_2 by reaction with graphite at 500°C, the CO_2 produced was absorbed by liquid nitrogen and was then analyzed by a Finnigan MAT Delta S mass spectrometer. The standard NBS-28 used in this study gave a $\delta^{18}O_{V\text{-}SMOW}$ value of 9.65 ± 0.15‰. The xenolith LW0006 (of which the analyzed portion is mainly composed of orthopyroxenite) gave $\delta^{18}O_{V\text{-}SMOW}$ values of 6.8‰ and 7.0‰, respectively, for two parallel samples.

5. Geochemistry and Isotopic Composition

[20] Xenolith LW0006 has higher concentrations of SiO_2 (46.01 wt%), Al_2O_3 (5.14 wt%), CaO (2.17 wt%), K_2O (0.67 wt%), Na_2O (0.65 wt%), and TiO_2 (0.26 wt%), and lower concentrations of MgO (34.25 wt%) than peridotite xenoliths of the Tietonggou and Cenozoic in Shandong province (Figure 9). The Na_2O, K_2O, and Al_2O_3 concentrations of xenolith LW0006 are also higher than those of pyroxenite xenoliths from Tietonggou.

[21] In a primitive mantle-normalized spider diagram, xenolith LW0006 shows a strong enrichment of Cs, Rb, Ba, Th, U, K, La and Ce relative to Nb and Ta, a strong positive anomaly in Pb (about 600 times that of primitive mantle), a small positive anomaly in Sr, strong negative anomalies in Nb, Ta, and small negative anomalies in P, Ti (Figure 10a). Ba is less enriched than Rb and Th. The total REE concentrations of this sample are comparable to those of pyroxenite xenoliths from Tietonggou, but are higher than those of peridotite xenoliths from Tietonggou (Figure 10b). In a chondrite-normalized REE diagram, all Tietonggou xenoliths show enrichments of the light rare earth elements (LREE) relative to heavy rare earth elements (HREE), which are distinct from those of Cenozoic mantle xenoliths in the Shandong province (Figure 10b).

[22] Xenolith LW0006, as well as other ultramafic xenoliths from Tietonggou, are characterized with enriched Sr-Nd isotopic compositions (Figure 11).

Table 5. Sr-Nd-Pb Isotopic Composition of Xenolith LW0006[a]

Rb	Sr	$^{87}Rb/^{86}Sr$	$^{87}Sr/^{86}Sr$ (2σ)	$^{87}Sr/^{86}Sr_i$	$\varepsilon_{Sr(T)}$		
28.35 ppm	176.4 ppm	0.4642	0.706954(29)	0.706129	25.3		
Sm	Nd	$^{147}Sm/^{144}Nd$	$^{143}Nd/^{144}Nd$(2σ)	$^{143}Nd/^{144}Nd_i$	$\varepsilon_{Nd(T)}$	T_{DM}	$f_{Sm/Nd}$
1.07 ppm	5.78 ppm	0.1120	0.512213(8)	0.512121	−6.9	1402 Ma	−0.43
$^{206}Pb/^{204}Pb$	$^{207}Pb/^{204}Pb$	$^{208}Pb/^{204}Pb$	$^{206}Pb/^{204}Pb_i$	$^{207}Pb/^{204}Pb_i$	$^{208}Pb/^{204}Pb_i$	Δ7/4	Δ8/4
17.164	15.410	37.534	17.151	15.409	37.521	5.9	116.1

[a] Initial values were calculated at 125 Ma.

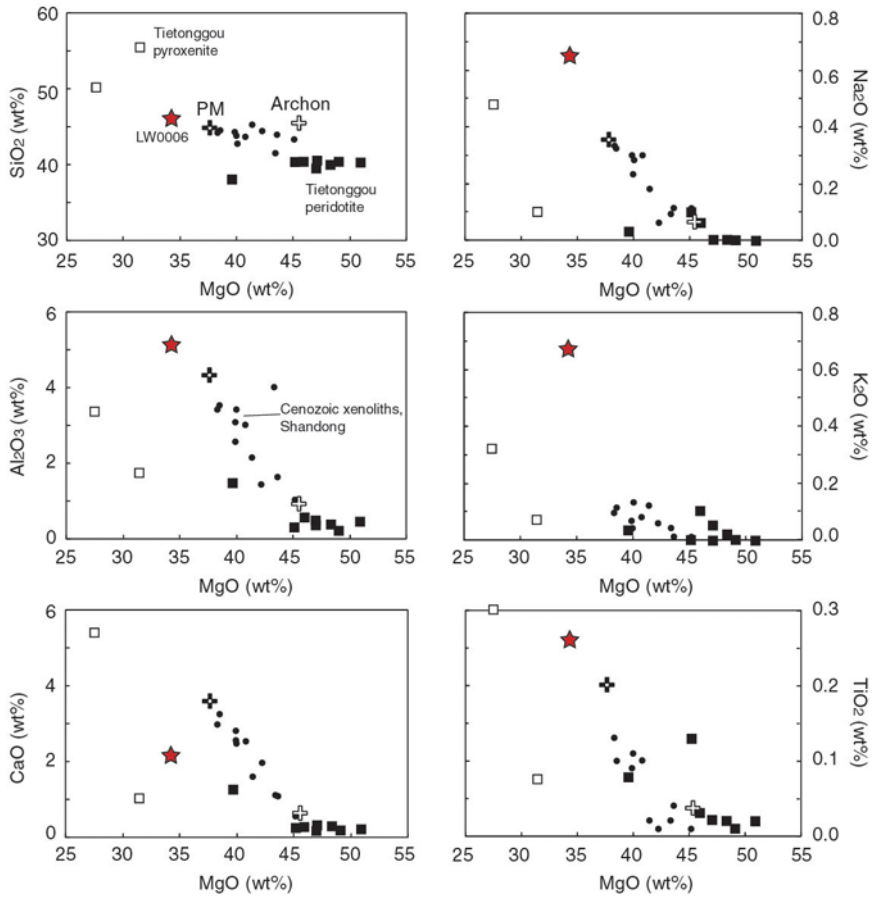

Figure 9. Major element composition of xenolith LW0006. Data for peridotite xenoliths from Cenozoic basalts of Shandong province are from *Rudnick et al.* [2004]. Data of other ultramafic xenoliths of Tietonggou are from *Chen and Zhou* [2004] and *Xu et al.* [2004a]. Archon is the average SCLM of the Archean craton [*Griffin et al.*, 2003]. PM is primitive mantle from *McDonough and Sun* [1995].

On a $^{87}Sr/^{86}Sr$ versus $^{143}Nd/^{144}Nd$ diagram, the range of Tietonggou xenoliths is distinct from that of Cenozoic basalts and their entrained xenoliths in Shandong province (Figure 11a), but is similar to that of their host rocks (Figure 11b). The lead isotopic composition of this sample, $^{206}Pb/^{204}Pb$ = 17.164, is less radiogenic than the Cenozoic basalts in Shandong province ($^{206}Pb/^{204}Pb$ = 17.60 – 18.46 [*Peng et al.*, 1986]), but more radiogenic than Ji'nan gabbros ($^{206}Pb/^{204}Pb$ = 16.62 – 16.94 [*Zhang et al.*, 2004]).

[23] The $\delta^{18}O$ value of xenolith LW0006 (6.9‰ average) is significantly higher than typical mantle xenoliths 4.8–5.5‰ [*Mattey et al.*, 1994] and typical MORB (5.2–6.1‰ [*Ito et al.*, 1987; *Eiler et al.*, 2000]). Until now, unusually elevated $\delta^{18}O$ values for direct mantle samples have only been found in mantle xenoliths from arc volcanics ($\delta^{18}O$ up to 11.3‰ [*Eiler et al.*, 1998]).

6. Discussion

6.1. Xenolith LW0006: An Extreme Example of Ultramafic Xenoliths Entrained in the Early Cretaceous Diorite of NCC

[24] The metasomatism observed in xenolith LW0006, has also been found in peridotite xenoliths of Tietonggou [*Chen and Zhou*, 2004], e.g., (1) disseminated phlogopite and clinopyroxene which are partially replaced by late-stage orthopyroxene, Na-rich plagioclase, and Na-rich amphibole, (2) phlogopite- and amphibole-bearing clinopyroxenite veinlets, (3) Na-rich amphibole- and plagioclase-bearing orthopyroxenite veinlets. Orthopyroxenite veinlets have been found in most

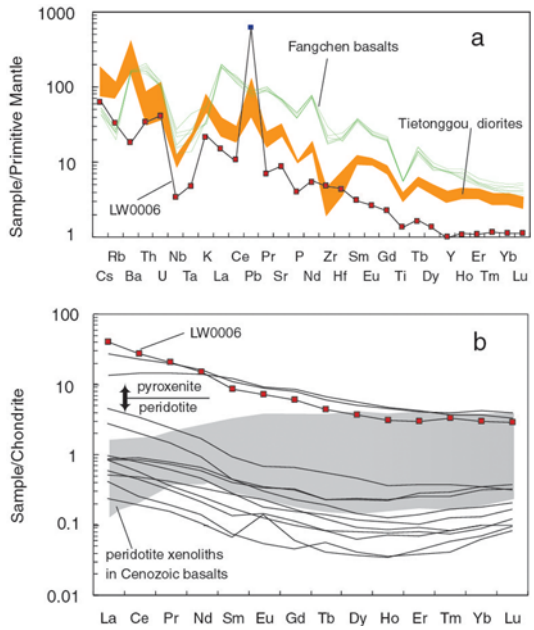

Figure 10. (a) Spider gram of xenolith LW0006, normalized to the values of the primitive mantle [*McDonough and Sun*, 1995], compared with the host diorites [*Chen*, 2001] and Fangchen basalts [*Zhang et al.*, 2002]. (b) REE pattern of xenolith LW0006 and other ultramafic xenoliths of Tietonggou [*Chen and Zhou*, 2004; *Xu et al.*, 2004a], compared with the mantle xenoliths in Cenozoic basalts of Shandong province [*Fan et al.*, 2000]. REE concentrations are normalized to the chondritic values of *Anders and Grevesse* [1989]. For the concentrations of trace elements in the Cenozoic xenoliths, $C_w = C_{cpx} \times$ modal percent of cpx, where C_w is the element concentration for the whole rock (shown in the figure) and C_{cpx} is the element concentration for clinopyroxene.

peridotite xenoliths from Tietonggou. Several orthopyroxenite veinlets can be observed in those large peridotite xenoliths. The mineral chemistry of this xenolith, such as the low Al_2O_3 concentrations of secondary orthopyroxene, is consistent with other Tietonggou xenoliths (Figure 8). The enrichment of LREE relative to HREE of this xenolith is also a common characteristic in Tietonggou xenoliths (Figure 10b) and the Sr-Nd isotopic composition of this xenolith does not differs too much from that of other Tietonggou xenoliths (Figure 11). Therefore xenolith LW0006, the most extremely metasomatized sample found so far in the xenolith suite of Tietonggou, provides the opportunity to better constrain the source and environment of this metasomatism, which may have been pervasive in the lithospheric mantle of this age. Since the mineral compositions of the orthopyroxenite portion of this xenolith are similar with those orthopyroxenite veinlets in peridotite xenoliths of Tietonggou, the orthopyroxenite of this xenolith may be a thick melt channel. *Xu et al.* [2003a] reported that disseminated phlogopite with secondary orthopyroxene and veinlets composed of phlogopite, orthopyroxene, and plagioclase can be observed in dunite xenoliths in the Jin'lin

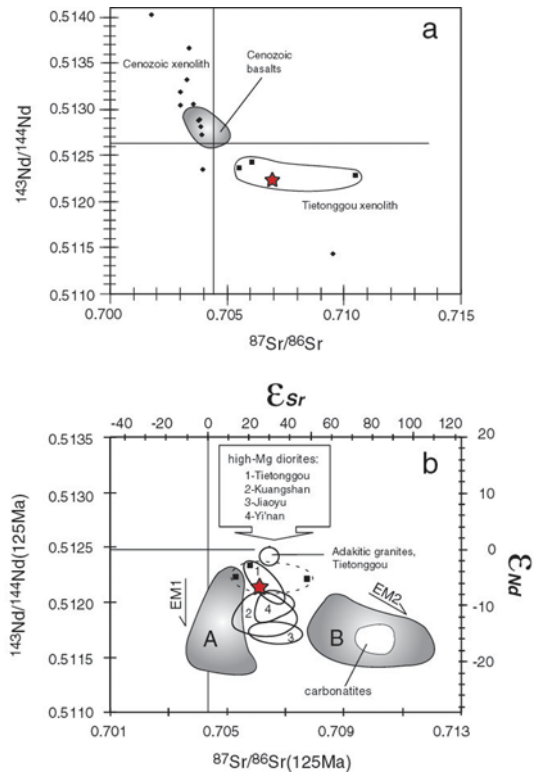

Figure 11. Sr-Nd isotopic composition of xenolith LW0006. (a) Present value of $^{87}Sr/^{86}Sr$ versus $^{143}Nd/^{144}Nd$. (b) Initial value of $^{87}Sr/^{86}Sr$ versus $^{143}Nd/^{144}Nd$. Star, xenolith LW0006; squares, other ultramafic xenoliths of Tietonggou [*Chen and Zhou*, 2004]; diamond, mantle xenoliths in Cenozoic basalts of Shandong province [*Fan et al.*, 2000]; all Cenozoic xenoliths plot in the second square except for two pyroxenite xenoliths. Cenozoic basalts, Cenozoic basalts from Shandong province [after *Peng et al.*, 1986]; A, Cretaceous gabbros and basalts from the northern part of west Shandong province [*Guo et al.*, 2001, 2003; *Zhang et al.*, 2003]; B, Cretaceous basalts and andesites from the southern part of west Shandong province [*Zhang et al.*, 2002; *Ying*, 2002; *Qiu et al.*, 2002]; carbonatites, Cretaceous carbonatites from Laiwu and Zibo [*Ying et al.*, 2004]. High-Mg diorites: 1, Tietonggou pluton [*Chen*, 2001]; 2, Kuangshan pluton [*Chen*, 2001]; 3, Jiaoyu pluton [*Xu et al.*, 2004]; 4, Yi'nan pluton [*Xu et al.*, 2004]. Note that two samples with obvious crustal contamination are not included in this figure and Figure 14. Adakitic granites from Tietonggou are from unpublished data of Chen.

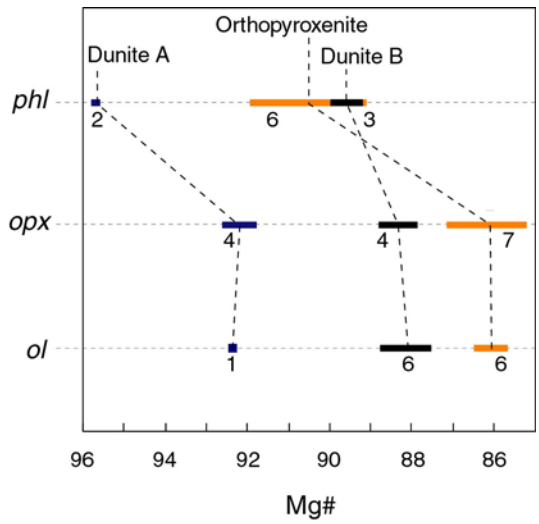

Figure 12. Mg-Fe disequilibrium of minerals in xenolith LW0006. Orthopyroxene and phlogopite show Mg-Fe equilibration with olivine in dunite A and dunite B but not in the orthopyroxenite, as seen by the broad range of Mg# values of phlogopite and orthopyroxene. Analytical numbers are shown by the line.

high-Mg diorite, an Early Cretaceous pluton in Zibo, west Shandong province. They suggested that these xenoliths might have been metasomatized by some kind of Si- and K-rich liquids. We speculate that the phlogopite might exist before the growth of the secondary orthopyroxene and plagioclase, and we will discuss similar metasomatic phenomena found recently in Tietonggou xenoliths late. Hence ultramafic xenoliths from the Tietonggou diorite of Laiwu and the Jin'lin diorite of Zibo might have undergone similar metasomatism to that observed in xenolith LW0006.

6.2. Interactions Between Xenolith and Host Magma

[25] Since the host diorite is Si-oversaturated, metasomatism observed in the xenolith, especially the growth of secondary orthopyroxene could result from interactions between the dioritic magma and the Si-undersaturated peridotite. Tietonggou xenoliths are frequently covered with thin hornblendite selvages. A hornblendite selvage also has been observed in the dunite portion of xenolith LW0006 (Figure 4b), which might be produced by reaction between the host magma and the dunite. The sharp boundary between the host diorite and the orthopyroxenite portion of xenolith LW0006 suggests there might be little reaction between them, since orthopyroxene and phlogopite are Si-saturated. The selvage and veinlet of hornblendite are common in some peridotite xenoliths carried by calc-alkaline andesites [*Arai et al.*, 2003a]. Since the host magma is a highly Si-oversaturated hydrous melt and olivine is highly Si-undersaturated, the reaction between them might produce hornblende quickly at the margin of the xenoliths at shallow depth, which would hamper further reaction between them. Therefore the metasomatism observed in Tietonggou xenoliths must have occurred before the entrainment by the host dioritic magma. The chemical differences between the metasomatic minerals in the xenoliths and the minerals in the host diorite, e.g., plagioclase, support this interpretation.

6.3. Metasomatic History

[26] The resorbed shapes of the dunite portions (Figure 2) suggest that the primary lithology of the composite xenolith is dunite, and that a series of metasomatism changed the composition of this specimen resulting in an orthopyroxenite-dominated lithology.

[27] In dunite A, the presence of the composite veinlet (clinopyroxenite + orthopyroxenite) suggests two stages of metasomatism occurring in the same path (Figure 5). The spatial relationship of the different parts of the composite veinlet and the exsolution textures of minerals suggest that the phlogopite- and amphibole-bearing clinopyroxenite veinlet was produced first. A second-stage of metasomatism consumed the early metasomatic minerals and produced the secondary orthopyroxene in the same passage. Mg# values of the secondary orthopyroxene (Mg# = 91.8 – 92.6) are similar to those of the olivine by the orthopyroxenite veinlet (Mg# = 92.3), which suggests that there has been Mg-Fe equilibration (Figure 12).

[28] In dunite B, the replacement relationship between clinopyroxene, phlogopite and orthopyroxene, amphibole, plagioclase suggests that there are at least two stages of metasomatism (Figure 6). Intergranular clinopyroxene and phlogopite were produced by early stage(s) of metasomatism. The later metasomatic event followed the same path as the early metasomatism, and affected the early stage metasomatic minerals, crystallizing orthopyroxene, amphibole, and plagioclase. The similar Mg# values of secondary orthopyroxene and primary olivine, 88.1–88.7 and 88.2, respectively, suggest that they have experienced Mg-Fe equilibration (Figure 12).

[29] All of minerals in the clinopyroxenite of the composite veinlet in Dunite A are enriched in CaO, which suggests that the metasomatic medium was a Ca-rich liquid, such as, e.g., carbonatite melts. The presence of phlogopite in the clinopyroxenite veinlet suggests that this metasomatic agent was also enriched in K. The intergranular minerals in dunite B also include phlogopite and clinopyroxene, which suggests that dunite B was also metasomatized by a K- and Ca-rich liquid. The high concentrations of K_2O (0.67 wt%) and CaO (2.17 wt%) in the whole rocks suggest that such metasomatism contribute significantly to the chemistry of the orthopyroxenite. The late-stage metasomatism in both dunite A and dunite B are characterized by the growth of secondary orthopyroxene, which suggests that both dunite A and dunite B were metasomatized by Si-rich liquids. Figure 7 shows that the late metasomatism in this part is characterized by the breakdown of phlogopite, the resorption of olivine, and the growth of orthopyroxene and plagioclase, which is consistent with what is seen in dunite A and dunite B. The growth of Na-rich plagioclase and Na-rich amphibole, as well as the high Na_2O concentration (0.65 wt%) of the whole rock, suggests that the late-stage metasomatic liquids were also enriched in Na_2O. Therefore we designate the late-stage metasomatism in the xenolith as Si (Na) metasomatism.

[30] Figure 12 illustrates that phlogopite and orthopyroxene in dunite A and dunite B have experience Mg-Fe equilibration with olivine, although this has not taken place in the orthopyroxenite. In the orthopyroxenite, olivine has a narrow range of Mg# values (85.5–86.6), whereas both phlogopite and orthopyroxene have broad ranges of Mg# values, 89.1–92.0 and 85.2–87.9, respectively. We have calculated that the equilibration temperatures of Tietonggou xenoliths are in the range of 690–790°C according to the orthopyroxene Ca thermometer [*Brey and Kohler*, 1990] and the olivine-spinel Mg-Fe exchange thermometer [*Fabries*, 1979; *Chen and Zhou*, 2004]. Under such high-temperature conditions, Mg-Fe exchange between silicate minerals is very rapid and it is easy to obtain Mg-Fe equilibrium in a short time. Therefore the Mg-Fe disequilibrium observed in the orthopyroxenite indicates that Si (Na) metasomatism may have occurred shortly before entrainment of the xenolith in the host magma. The Mg-Fe equilibrium observed in dunite A and dunite B may be due to low orthopyroxene/phlogopite:olivine ratios. It is reasonable to speculate that the ubiquitous heterogeneity of spinel also resulted from Si (Na) metasomatism.

[31] In summary, the petrography, mineral chemistry, and major element compositions provide a clear metasomatic record of the composite xenolith: K (Ca) metasomatism, and Si (Na) metasomatism. K (Ca) metasomatism is characterized by the development of phlogopite-, and amphibole-bearing clinopyroxenite veinlets or intergranular phlogopite (and clinopyroxene). Si (Na) metasomatism is characterized by the growth of secondary orthopyroxene, Na-rich plagioclases (with or without Na-rich amphibole), and the resorption of olivine and decomposition of phlogopite. Si (Na) metasomatism occurred shortly before entrainment of the xenolith. Tietonggou xenoliths are thought to be samples from the crust-mantle transitional zone (Moho) [*Chen and Zhou*, 2004] or uppermost mantle [*Xu et al.*, 2003b, 2004a]. Deep source-derived liquids, which metasomatized this region, might have metasomatized the entire SCLM.

6.4. Subduction-Related Metasomatism: Fluids Versus Melts

[32] The exceptional $\delta^{18}O$ value and exceptionally high concentrations of Na_2O, K_2O and Al_2O_3 in this sample suggest a clear contribution of recycled crust materials in the source. The elemental signatures of the orthopyroxenite portion of the xenolith, such as depletions of Nb, Ta, Ti, and P, and the positive Pb anomaly (Figure 10a), are similar to those of arc volcanics, which suggest that at least one of these three metasomatic events is related to subduction. Since the orthopyroxenite is mainly composed of secondary orthopyroxene, Si (Na) metasomatism is the most likely candidate to contribute to the elevated $\delta^{18}O$ value.

[33] In recent years, subduction-related metasomatism has become better understood through increased xenolith localities in arc settings, where ultramafic xenoliths have been thought to be fragments from a mantle wedge. These localities include the Japanese island arcs [*Abe et al.*, 1998; *Arai and Kida*, 2000], the Luzon arc of Philippines [*Maury et al.*, 1992; *Schiano et al.*, 1995; *Arai and Kida*, 2000; *Arai et al.*, 2004], the Colorado Plateau [*Smith and Riter*, 1997; *Smith et al.*, 1999], the Cascades, USA [*Brandon and Draper*, 1996; *Ertan and Leeman*, 1996; *Brandon et al.*, 1999], Mexico [*Luhr and Aranda-Gómez*, 1997; *Blatter and Carmichael*, 1998], Papua New Guinea [*McInnes and Cameron*, 1994; *Grégoire et al.*, 2001; *McInnes et al.*, 2001; *Franz et al.*, 2002],

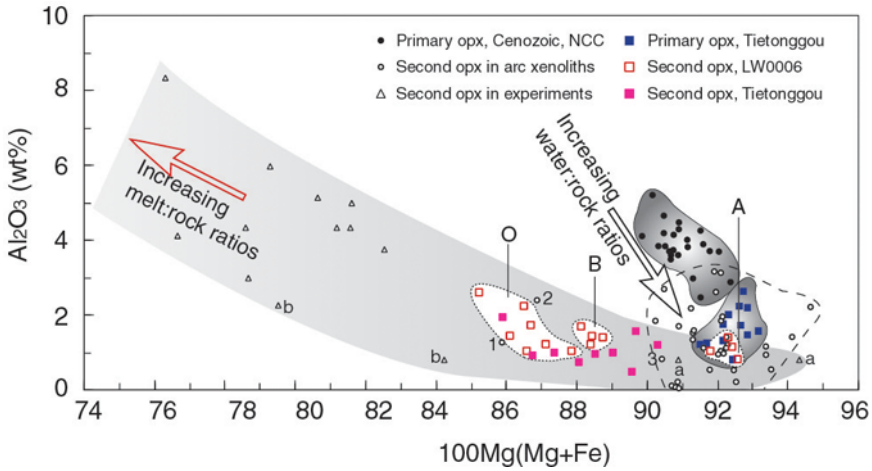

Figure 13. Comparison of the compositions of orthopyroxene (opx) in mantle xenoliths with different tectonic backgrounds. A, opx in Dunite A of xenolith LW0006; B, opx in Dunite B of xenolith LW0006; O, opx in the orthopyroxenite of xenolith LW0006. Primitive opx from Tietonggou xenoliths (this study) show more depleted compositions than Cenozoic xenoliths of the NCC [*Rudnick et al.*, 2004]. Secondary opx from Tietonggou xenoliths have low Al_2O_3 signatures, which is similar to those of arc xenoliths, but they have clearly lower Mg# values than most arc samples. Such signatures have only been found in a few cases, such as 1, daughter mineral inside high-silica glass inclusions in harzburgitic olivine [*Schiano et al.*, 1995]; 2, metasomatic orthopyroxenite [*Ertan and Leeman*, 1996]; and 3, Quartz diorite veins in lherzolite [*Arai et al.*, 2003b]. Orthopyroxene crystallized in the reaction experiments between silica-rich melts and peridotites/olivines: a, 15 kbar, 900°C and 1000°C, mixture of 60 wt% trondhjemite and 40 wt% olivine, and 7.8 wt% an 9.6 wt% H_2O added [*Prouteau et al.*, 2001]; b, 3.8 Gpa, 1100°C and 1150°C, reaction between partial melts from amphibolitized pillow lava and 16 wt% and 30 wt% depleted peridotite [*Rapp et al.*, 1999]; other triangles, 850–1100°C, 15 kbar, mixture of 95 wt%, 90 wt% tonalite and 5 wt%, 10 wt% peridotite, and 5–10 wt% H_2O added [*Carroll and Wyllie*, 1989].

Southern Patagonia, Argentina [*Gorring and Kay*, 2000; *Laurora et al.*, 2001], the Canadian Cordillera [*Peslier et al.*, 2002], Kamchatka [*Kepezhinskas et al.*, 1995; *Arai et al.*, 2003a], and the Betic Cordillera, southern Spain [*Arai et al.*, 2003b; *Beccaluva et al.*, 2004]. Mantle xenoliths from these localities show complicated modal metasomatism, including vein metasomatism, pervasive metasomatism and irregular metasomatism. Some silica-rich glass inclusions, pockets and veinlets have been also found in these mantle xenoliths as residue melts [*Schiano et al.*, 1995; *Ertan and Leeman*, 1996; *Eiler et al.*, 1998]. These wedge-derived samples provide direct evidence that slab-derived fluids/melts have modified the mantle wedge and have affected the geochemical characteristics of arc volcanics.

[34] Among these wedge-derived samples, secondary orthopyroxenes are common and have been thought to be a mark of Si metasomatism in the subarc mantle. Secondary orthopyroxenes are characterized by a depletion of Al_2O_3 relative to primitive orthopyroxene. The crystallization of orthopyroxenes suggests that the metasomatic liquids are saturated with silica. Up to now, it has been controversial whether such slab-derived silica-rich liquids are fluids or melts. *McInnes et al.* [2001] found that orthopyroxenes in fluid-metasomatized peridotites are enriched in Mg# and depleted in Al_2O_3 compared to anhydrous peridotite, and this trend correlates with an increase in the intensity of fluid:rock interactions. In Figure 13, we illustrate the published chemical data of orthopyroxenes in metasomatized peridotite xenoliths from arc settings, and find that such a trend appears in orthopyroxenes in most cases (Mg# > 90). In addition, orthopyroxenes with low Mg# values (85–87) have been found in a few cases, including daughter minerals inside silica-rich melt inclusions in olivine from Philippines xenoliths (Schiano et al. 1995) and orthopyroxenes in an intensely metasomatized xenolith, with many silica-rich melt inclusions and pockets from the Cascades, USA (Ertan and Leeman, 1996). Petrographic evidence shows that there are genetic relationships between low-Mg# orthopyroxenes and silica-rich melt inclusions. *Carroll and Wyllie* [1989], *Rapp et al.* [1999], and *Prouteau et al.* [2001] carried out a series of experiments on the interactions between silica-rich melts and peridotites/olivines. These experiments show a clear correlation between the

composition of the secondary orthopyroxenes and the melt:rock ratios. Mg# values of the secondary orthopyroxenes decrease and their Al_2O_3 concentrations increase with increased melt:rock ratios, so that low-Mg# orthopyroxenes are formed under high melt:rock ratio conditions (Figure 13). Thus we propose that the growth of low-Mg# orthopyroxene in mantle wedge results from intense metasomatism by slab-derived melts.

[35] The secondary orthopyroxene of Tietonggou xenoliths is also characterized by low Al_2O_3 concentrations (Figure 8). In xenolith LW0006, secondary orthopyroxene shows broad range of compositions. Orthopyroxene in the orthopyroxenite has lower Mg# values (85.2–87.9) than dunite A (91.8–92.6) and dunite B (88.1–88.7). In Figure 13, orthopyroxenes from the three parts of xenolith LW0006 fall within the experimental range of melt:rock interactions and display the same general trend, which is distinct from the trend suggested for fluid:melt interaction. *Arai et al.* [2003a] noted that fluid metasomatism is characterized by simple mineral compositions and complicated boundaries between secondary orthopyroxene and primary minerals. In contrast, the metasomatic minerals in xenolith LW0006 not only include orthopyroxene, but also plagioclase, amphibole, zircon, rutile, apatite, etc., which could not have crystallized from fluids. The simple boundaries between secondary orthopyroxene and primary olivine also support melt-induced metasomatism. Consequently, the Si (Na) metasomatic liquids of the Tietonggou xenoliths most likely are slab-derived melts, and not fluids.

[36] Na metasomatism had been recognized in mantle xenoliths from the north Kamchatka arc and is characterized by the growth of Na-rich clinopyroxene and Na-rich plagioclase [*Kepezhinskas et al.*, 1995]. The occurrence of trondhjemitic veins in the xenoliths suggests that these metasomatic liquids are adakitic melts from partial melting of subducted oceanic crust [*Kepezhinskas et al.*, 1995]. Thus the growth of Na-rich plagioclase in Tietonggou xenoliths also suggests that the late-stage metasomatic liquids might be slab-derived melts.

6.5. Metasomatism and Heterogeneity of the SCLM Beneath Shandong Province

[37] Mantle-derived rocks of the Early Cretaceous are prevalent in Shandong province and provide a window to understand the chemical composition of the SCLM beneath this region. In Figure 11b, we illustrate the Sr-Nd isotopic composition of these rocks and divide them into three suites: series A, series B, and series C. Series A includes gabbros and basalts from the northern part of west Shandong (Ji'nan, Zhangqiu, and Zoupin); they have low $^{87}Sr/^{86}Sr$ (0.70396–0.70580) and low $^{143}Nd/^{144}Nd$ (0.51140–0.51228) [*Guo et al.*, 2001, 2003; *Zhang et al.*, 2004]. Series B includes basalts, andesites, and lamprophyres from east Shandong and the southern part of west Shandong, and carbonatites of Laiwu and Zibo, with high $^{87}Sr/^{86}Sr$ (0.70609–0.71177) and low $^{143}Nd/^{144}Nd$ (0.51149–0.51205) [*Zhang et al.*, 2002; *Qiu et al.*, 2002; *Ying et al.*, 2004; *Yang et al.*, 2004]. Series C are the high-Mg diorite-dominated plutons in west Shandong, which have higher $^{143}Nd/^{144}Nd$ ratios (0.51167–0.51247) and moderate $^{87}Sr/^{86}Sr$ ratios (0.70529–0.70740) [*Chen*, 2001; *Xu et al.*, 2004]. Therefore these three series of rocks can be distinguished by their $^{87}Sr/^{86}Sr$ ratios.

[38] The SCLM beneath Archean cratons is generally characterized by enriched Sr-Nd isotopic signatures, such as Kapavaal [*Walker et al.*, 1989], Wyoming [*Carlson and Irving*, 1994], and Siberia [*Pearson et al.*, 1995]. Archean mantle with low abundances of phlogopite (low phlogopite/clinopyroxene ratios) can evolve into a mantle with a low $^{87}Sr/^{86}Sr$ and low $^{143}Nd/^{144}Nd$ signature, as Rb is fixed in phlogopite whereas Sr, Nd, and Sm are mainly incorporated into clinopyroxene [*Schimidt et al.*, 1999]. Such a Sr-Nd isotopic signature can be found in Early Cretaceous rocks not only from Shandong province, but also many other areas in the NCC, such as the Taihang area, the Yanshan area and the north margin of NCC. *Guo et al.* [2003] proposed that the SCLM beneath the NCC is characterized by the same isotopic signature, and that mafic rocks with this Sr-Nd isotopic signature, shown as series A in Figure 8b, originate from the uppermost part of an aged and refractory SCLM with a low phlogopite/clinopyroxene ratio. Early Cretaceous rocks with high $^{87}Sr/^{86}Sr$ and low $^{143}Nd/^{144}Nd$, shown as series B in Figure 11b, are more typical in Shandong province. The mantle sources for these rocks might have been enriched by the subduction of the Yangtze craton [*Qiu et al.*, 2002; *Zhang et al.*, 2002; *Ying et al.*, 2004] or ancient subduction events [*Yang et al.*, 2004]. It is significant that Laiwu-Zibo carbonatites and Fangcheng basalts not only have extremely enriched Rb, Ba, U and LREE (Figure 10a), but also have high CaO concentrations, 19.6–46.9 wt% and 8.7–10.0 wt%, respectively. Since the REE are mainly incorporated in clinopyroxene whereas Rb, Ba, U are fixed in phlogopite and amphiboles in the upper mantle, it is

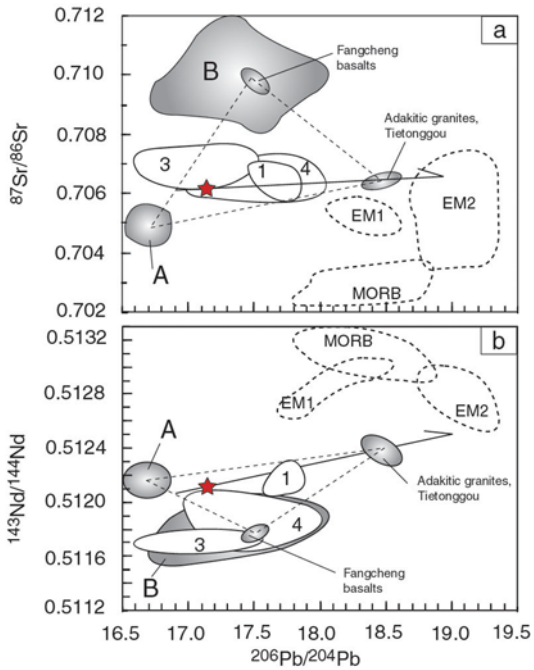

Figure 14. Initial value of $^{206}Pb/^{204}Pb$ versus that of $^{87}Sr/^{86}Sr$ and $^{143}Nd/^{144}Nd$. Symbols and data sources are the same as in Figure 11. Note that the data of series A here include only the Ji'nan gabbros [*Zhang et al.*, 2004]. The fields of MORB, EM1, and EM2 are taken from *Zou et al.* [2000]. In Figure 14a, all high-Mg diorites are shown in the triangular field outlined by dashes, composed of series A, series B, and adakitic granites. Mixing of adakitic granites (with high $^{206}Pb/^{204}Pb$ and high $^{143}Nd/^{144}Nd$) and a source with low $^{206}Pb/^{204}Pb$ and $^{143}Nd/^{144}Nd$ (such as, e.g., series A or a mixing between series A and series B) can produce high-Mg diorites.

reasonable to deduce that the source for series B is vein-plus-peridotite mantle with amphibole- or phlogopite-bearing clinopyroxenite veins [*Yang et al.*, 2004]. Thus the K (Ca) metasomatism observed in Tietonggou xenoliths might be associated with the enriched Sr-Nd isotopic signature of the SCLM beneath the NCC.

[39] Tietonggou diorites, as well as other high-Mg diorites in west Shandong province [*Chen*, 2001; *Xu et al.*, 2004], have low SiO_2 (57–60 wt%), high MgO (>6 wt%) and Mg# values (>0.7), high concentrations of Cr (>500 ppm) and Ni (>150 ppm), enrichments in Sr (>600 ppm) and Ba (>1000 ppm), and high Na_2O (3.1–3.4 wt%), K_2O (1.8–2.4 wt%), LREE, and La/Yb_N ratios (>10) [*Chen*, 2001]. The geochemical characteristics of Tietonggou diorites are similar to those of sanukitoids and low-SiO_2 adakites, which are thought to be partial melts from a mantle wedge whose composition has been modified by reaction with slab melts (see review by *Martin et al.* [2005]). Besides high-Mg diorites, granitic rocks also exist in the Tietonggou pluton. Tietonggou granites have high SiO_2 (70.5–72.0 wt%), high Na_2O (4.5–5.2 wt%), $Na_2O/K_2O > 1$, high Sr (590–670 ppm), high La/Yb_N (50–100), and extremely depleted HREE (Yb < 0.3 ppm) and Y (<4 ppm) (unpublished data of Chen). The geochemical characteristics of Tietonggou granites are similar to those of high-SiO_2 adakites, which are broadly thought to be slab melts [*Martin et al.*, 2005]. Thus geochemical evidence from the Tietonggou pluton also indicates that the SCLM beneath Laiwu might have been metasomatized by slab melts.

[40] In $^{206}Pb/^{204}Pb$ versus $^{87}Sr/^{86}Sr$ and $^{143}Nd/^{144}Nd$ diagrams, adakitic granites, high-Mg diorites, and xenolith LW0006 of Tietonggou line up along a possible mixing array (Figure 14). The isotopic composition of xenolith LW0006 and its host rocks can be produced by mixing between an enriched mantle with low $^{206}Pb/^{204}Pb$ and low $^{143}Nd/^{144}Nd$, and the adakitic granites with high $^{206}Pb/^{204}Pb$ and high $^{143}Nd/^{144}Nd$. It is evident that other high-Mg diorite-dominated plutons also plot along the possible mixing line of Tietonggou in the $^{206}Pb/^{204}Pb$ versus $^{87}Sr/^{86}Sr$ diagram (Figure 14a), but plot under the possible mixing line of Tietonggou in the $^{206}Pb/^{204}Pb$ versus $^{143}Nd/^{144}Nd$ diagram (Figure 14b). Each high-Mg diorite-dominated pluton has a broad range of $^{206}Pb/^{207}Pb$ ratios. Since high-Mg diorites are exceptionally enriched in Sr, crustal assimilation might have less of an affect on their Sr isotopes than their Nd and Pb isotopes. Therefore high-Mg diorites in west Shandong province might have a similar source as the high-Mg diorites of Tietonggou, which were metasomatized by slab melts like adakitic granites of Tietonggou. *Xu et al.* [2003b, 2004a, 2004c] suggested that the metasomatic agent for Tietonggou xenoliths might be from a recycled continental crust. However, the higher $^{143}Nd/^{144}Nd$ ratios of adakitic granites, high-Mg diorites of Tietonggou than of other Early Cretaceous mantle-derived rocks in Shandong province do not support such a proposal (Figures 11b and 14b). Thus Si (Na) metasomatism observed in Tietonggou xenoliths provides direct evidence for the genesis of high-MgO diorites in Shandong province.

6.6. Relationship Between Subduction and Lithospheric Transformation

[41] Dating the Mesozoic rocks could provide a temporal framework for the lithosphere thinning.

Xu et al. [2004] summarized the reliable ages of Mesozoic mafic rocks and felsic rocks in the NCC, and found that they clustered around 130 Ma, which is consistent with the time of gold mineralization [*Yang et al.*, 2003; *Zhou et al.*, 2002] and the peak age of granulite xenoliths [*Wilde et al.*, 2003]. Thus the peak stage of lithospheric thinning has generously been thought to occur in the Early Cretaceous [*Menzies and Xu*, 1998; *Xu*, 2001; *Zhang et al.*, 2002, 2003, 2004; *Zhou et al.*, 2002; *Yang et al.*, 2003; *Guo et al.*, 2003; *Zhai et al.*, 2003; *Xu et al.*, 2004b, 2004c; *Xu et al.*, 2004; *Gao et al.*, 2004]. Some Jurassic rocks have also been found in the NCC recently [*Wilde et al.*, 2003; *Xu et al.*, 2004; *Gao et al.*, 2004], which suggests that the onset of the lithospheric thinning may be as early as the Early Jurassic. *Xu et al.* [2004] argue that the end of the lithospheric thinning is marked by the asthenosphere-derived basalts at about 70 Ma [*Yan et al.*, 2003]. Therefore the thinning of the SCLM beneath the NCC is a long-term process.

[42] The direct cause of lithospheric thinning of the eastern NCC is still controversial, and various models have been postulated, including thermal/chemical erosion or convective thinning [*Xu*, 2001; *Zhang et al.*, 2002; *Xu et al.*, 2004a, 2004c; *Xu et al.*, 2004], delamination induced by collision of the Yangtze Craton and the NCC [*Gao et al.*, 1998], or the effect of Pacific ocean subduction [*Tatsumoto et al.*, 1992], and mantle overturn [*Wilde et al.*, 2003]. As previously noted by others, mantle xenoliths from Cenozoic basalts have not provided direct evidence to test the foregoing hypotheses. The study of ultramafic xenoliths from high-Mg diorite-dominated plutons in NCC might provide important information on the thinning lithosphere, since the age of the high-Mg diorites is consistent with the peak stage of the lithospheric thinning. The above discussions show that Tietonggou xenoliths might have been metasomatized by slab melts shortly before entrainment of the xenoliths in the host magma, which indicates that ocean subduction might have been involved in the thinning process. High-Mg diorites and high-Mg andesites from the Early Cretaceous also have been found in the Japan arc [*Kamei et al.*, 2004; *Tsuchiya et al.*, 2005], which suggests that oceanic subduction modified the SCLM beneath the eastern margin of the Eurasian continent in the late Mesozoic. Thus the genetic relationship between oceanic subduction and reactivation of the old craton should be investigated farther.

7. Conclusions

[43] 1. Petrological evidence from a unique composite xenolith in Laiwu diorites reveals a complicated metasomatic history in the SCLM beneath the east NCC, including K (Ca) metasomatism as early stage enrichment, and Si (Na) metasomatism as a late event.

[44] 2. Evidence from the mineral chemistry, geochemistry, and Sr-Nd-Pb-O isotopic compositions of the unique xenolith indicate that Si (Na) metasomatism might result from reactions with slab melts, and occur shortly before entrainment by the host magma.

[45] 3. Si (Na) metasomatism observed in Tietonggou xenoliths, which are genetically linked with Early Cretaceous high-Mg diorites and adakitic granites in west Shandong, suggests that the SCLM beneath this area was modified by slab-derived melts. Since Si (Na) metasomatism occurred at the peak stage of the lithospheric thinning, subduction might have been involved in the thinning process of the SCLM beneath the NCC.

Acknowledgments

[46] This work was financially supported by the Chinese National Ministry of Science and Technology (grant G1999075504 to Zhou) and the National Natural Science Foundation of China (grant 40302014 to Chen). Oshiyuki Tatsumi and two anonymous reviewers provided constructive suggestions. Z.-Y. Chu assisted in the Sr-Nd-Pb isotope analyses. Analyses of oxygen isotopes were performed by T.-J. Li. G.-M. Su, R.-C. Wang, W.-R. Zhang, and X.-M. Chen assisted in the mineral analyses. Christine Floss improved the language in this manuscript.

References

Abe, N., S. Arai, and H. Yurimoto (1998), Geochemical characteristics of the uppermost mantle beneath the Japan island arc: Implications for upper mantle evolution, *Phys. Earth Planet. Inter.*, *107*, 233–248.

Anders, E., and N. Grevesse (1989), Abundances of the elements: Meteoritic and solar, *Geochim. Cosmochim. Acta.*, *53*, 197–214.

Arai, S., and M. Kida (2000), Origin of fine-grained peridotite xenoliths from Iraya volcano of Batan Island, Philippines: Deserpentinization or metasomatism at the wedge mantle beneath an incipient arc?, *Island Arc*, *9*, 458–471.

Arai, S., S. Ishimaru, and V. M. Okrugin (2003a), Metasomatized harzburgite xenoliths from Avacha volcano as fragments of mantle wedge of the Kamchatka arc: Implication for the metasomatic agent, *Island Arc*, *12*, 233–246.

Arai, S., Y. Shimizu, and F. Gervilla (2003b), Quartz diorite veins in a peridotite xenolith from Tallante, Spain: Implications for reaction and survival of slab-derived SiO_2-oversaturated melt in the upper mantle, *Proc. Jpn. Acad., Ser. B*, *79*, 145–150.

Arai, S., S. Takada, K. Michibayashi, and M. Kida (2004), Petrology of peridotite xenoliths from Iraya Volcano, Philippines, and its implication for dynamic mantle-wedge processes, *J. Petrol.*, *45*, 369–389.

Beccaluva, L., G. Bianchini, C. Bonadiman, F. Siena, and C. Vaccaro (2004), Coexisting anorogenic and subduction-related metasomatism in mantle xenoliths from the Betic Cordillera (southern Spain), *Lithos*, *75*, 67–87.

Blatter, D. L., and I. S. E. Carmichael (1998), Hornblende peridotite xenoliths from central Mexico reveal the highly oxidized nature of subarc upper mantle, *Geology*, *26*, 1035–1038.

Brandon, A. D., and D. S. Draper (1996), Constraints on the origin of the oxidation state of mantle overlying subduction zones: An example from Simcoe, Washington, USA, *Geochim. Cosmochim. Acta*, *60*, 1739–1749.

Brandon, A. D., H. Becker, R. W. Carlson, and S. B. Shirey (1999), Isotopic constraints on time scales and mechanisms of slab material transport in the mantle wedge: Evidence from the Simcoe mantle xenoliths, Washington, USA, *Chem. Geol.*, *160*, 387–407.

Brey, G. T., and T. Kohler (1990), Geothermobarometry in four phase lherzolites, part II: New thermobarometers, and practical assessment of existing thermobarometers, *J. Petrol.*, *31*, 1353–1378.

Carlson, R. W., and A. J. Irving (1994), Depletion and enrichment history of subcontinental lithospheric mantle: An Os, Sr, Nd and Pb isotopic study of ultramafic xenoliths from the northwestern Wyoming Craton, *Earth Planet. Sci. Lett.*, *126*, 457–472.

Carroll, M. R., and P. J. Wyllie (1989), Experimental phase relations in the system tonalite-peridotite-H_2O at 15 kb: Implication for assimilation and differentiation processes near the crust-mantle boundary, *J. Petrol.*, *30*, 1351–1382.

Chen, L. H. (2001), Genesis of high-Mg intrusions and their ultramafic xenoliths, Laiwu, Shandong Province, Eastern China (in Chinese), Ph.D. thesis, Inst. of Geol. and Geophys., Chin. Acad. of Sci., Beijing.

Chen, L. H., and X. H. Zhou (2004), Ultramafic xenoliths in Mesozoic diorites in west Shandong Province, *Sci. China, Ser. D*, *47*, 489–499.

Dong, Z. (1987), *Yanshanian Intrusive Complex of Central Shandong and Mineralization* (in Chinese), Geol. Publ., Beijing.

Eiler, J. M., B. McInnes, J. W. Valley, C. M. Graham, and E. M. Stolper (1998), Oxygen isotope evidence for slab-derived fluids in the sub-arc mantle, *Nature*, *393*, 777–781.

Eiler, J. M., P. Schiano, N. Kitchen, and E. M. Stolper (2000), Oxygen isotope evidence for recycled crust in the sources of mid-ocean ridge basalts, *Nature*, *403*, 530–534.

Ertan, I. E., and W. P. Leeman (1996), Metasomatism of Cascades subarc mantle: Evidence from a rare phlogopite orthopyroxenite xenolith, *Geology*, *24*, 451–454.

Fabries, J. (1979), Spinel-olivine geothermometry in peridotites from ultramafic complexes, *Contrib. Mineral. Petrol.*, *69*, 329–336.

Fan, W. M., H. F. Zhang, J. Baker, K. E. Jarvis, P. R. D. Mason, and M. A. Menzies (2000), On and off the North China Craton: Where is the Archaean keel?, *J. Petrol.*, *41*, 933–950.

Franz, L., K.-P. Becker, W. Kramer, and P. M. Herzig (2002), Metasomatic mantle xenoliths from the Bismarck Microplate (Papua New Guinea)—Thermal evolution, geochemistry and extent of slab-induced metasomatism, *J. Petrol.*, *43*, 315–343.

Gao, S., B.-R. Zhang, Z.-M. Jin, H. Kern, T.-C. Luo, and Z.-D. Zhao (1998), How mafic is the lower continental crust?, *Earth Planet. Sci. Lett.*, *161*, 101–117.

Gao, S., R. L. Rudnick, R. W. Carlson, W. F. McDonough, and Y. S. Liu (2002), Re-Os evidence for replacement of ancient mantle lithosphere beneath the North China craton, *Earth Planet. Sci. Lett.*, *198*, 307–322.

Gao, S., R. L. Rudnick, H.-L. Yuan, X.-M. Liu, Y.-S. Liu, W.-L. Xu, W.-L. Ling, J. Ayers, X.-C. Wang, and Q.-H. Wang (2004), Recycling lower continental crust in the North China craton, *Nature*, *432*, 892–897.

Gorring, M. L., and S. M. Kay (2000), Carbonatite metasomatized peridotite xenoliths from South Patagonia: Implications for lithosphere processing and Neogene plateau magmatism, *Contrib. Mineral. Petrol.*, *140*, 55–72.

Grégoire, M., B. I. A. McInnes, and S. Y. O'Reilly (2001), Hydrous metasomatism of oceanic sub-arc mantle, Lihir, Papua New Guinea Part 2. Trace element characteristics of slab-derived fluids, *Lithos*, *59*, 91–108.

Griffin, W. L., A. D. Zhang, S. Y. O'Reilly, and C. G. Ryan (1998), Phanerozoic evolution of the lithosphere beneath the Sino-Korean Craton, in *Mantle Dynamics and Plate Interactions in East Asia*, *Geodyn. Ser.*, vol. 27, edited by M. Flower et al., pp. 107–126, AGU, Washington, D. C.

Griffin, W. L., S. Y. O'Reilly, N. Abe, S. Aulbach, R. M. Davies, N. J. Pearson, B. J. Doyle, and K. Kivi (2003), The origin and evolution of Archean lithospheric mantle, *Precam. Res.*, *127*, 19–41.

Guo, F., W. M. Fan, Y. J. Wang, and G. Lin (2001), Late Mesozoic mafic intrusive complexes in North China block: Constraints on the nature of subcontinental lithospheric mantle, *Phys. Chem. Earth, Part A*, *26*, 159–771.

Guo, F., W. Fan, Y. Wang, and G. Ling (2003), Geochemistry of late Mesozoic mafic magmatism in west Shandong Province, eastern China: Characterizing the lost lithospheric mantle beneath the North China Block, *Geochem. J.*, *37*, 63–77.

Ito, E., W. M. White, and C. Goepel (1987), The O, Sr, Nd and Pb isotope geochemistry of MORB, *Chem. Geol.*, *62*, 157–176.

Jahn, B. M., B. Auvray, J. Comichet, Y. L. Bai, Q. H. Shen, and D. Y. Liu (1987), 3.5 Ga old amphibolites from eastern Hebei province China: Field occurrence, petrography, Sm-Nd isochron age and REE geochemistry, *Precam. Res.*, *34*, 311–346.

Jin, X., and H. Zhu (2000), Determination of 43 trace elements in rocks samples by double focusing high resolution inductively coupled plasma-mass spectrometry (in Chinese), *Chin. J. Anal. Chem.*, *28*, 563–567.

Kamei, A., M. Owada, T. Nagao, and K. Shiraki (2004), High-Mg diorites derived from sanukitic HMA magmas, Kyushu Island, southwest Japan arc: Evidence from clinopyroxene and whole rock compositions, *Lithos*, *75*, 359–371.

Kepezhinskas, P. K., M. J. Defant, and M. S. Drummond (1995), Na metasomatism in the island-arc mantle by slab melt-peridotite interaction: Evidence from mantle xenoliths in the north Kamchatka arc, *J. Petrol.*, *36*, 1505–1527.

Laurora, A., M. Mazzucchelli, G. Rivalenti, R. Vannucci, A. Zanetti, M. A. Barbieri, and C. A. Cingolani (2001), Metasomatism and melting in carbonated peridotite xenoliths from the mantle wedge: The Gobernador Gregores Case (Southern Patagonia), *J. Petrol.*, *42*, 69–87.

Liu, D.-Y., A. P. Nutman, W. Compston, J. S. Wu, and Q.-H. Shen (1992), Remnants of >3800 Ma crust in the Chinese part of the Sino-Korean craton, *Geology*, *20*, 339–342.

Luhr, J. F., and J. J. Aranda-Gómez (1997), Mexican peridotite xenoliths and tectonic terranes: Correlations among vent location, texture, temperature, pressure, and oxygen fugacity, *J. Petrol.*, *38*, 1075–1112.

Martin, H., R. H. Smithies, R. Rapp, J.-F. Moyend, and D. Champion (2005), An overview of adakite, tonalite-trondhjemite-granodiorite (TTG), and sanukitoid: Relationships and some implications for crustal evolution, *Lithos*, *79*, 1–24.

Mattey, D., D. Lowry, and C. Macpherson (1994), Oxygen isotope composition of mantle peridotite, *Earth Planet. Sc. Lett.*, *128*, 231–241.

Maury, R. C., M. J. Defant, and J.-L. Joron (1992), Metasomatism of the sub-arc mantle inferred from trace elements in Philippine xenoliths, *Nature*, *360*, 661–663.

McDonough, W. F., and S. S. Sun (1995), The composition of the Earth, *Chem. Geol.*, *120*, 223–253.

McInnes, B. I. A., and E. M. Cameron (1994), Carbonated, alkaline hybridizing melts from the sub-arc environment: Mantle wedge samples from the Tabar-Lihir-Tanga-Feni arc, Papua New Guinea, *Earth Planet. Sci. Lett.*, *122*, 125–141.

McInnes, B. I. A., M. Gregoire, R. A. Binns, P. M. Herzig, and M. D. Hannington (2001), Hydrous metasomatism of oceanic sub-arc mantle, Lihir, Papua New Guinea: Petrology and geochemistry of fluid-metasomatised mantle wedge xenoliths, *Earth Planet. Sci. Lett.*, *188*, 169–183.

Menzies, M. A., and Y. Xu (1998), Geodynamics of the North China Craton, in *Mantle Dynamics and Plate Interactions in East Asia*, *Geodyn. Ser.*, vol. 27, edited by M. Flower et al., pp. 155–165, AGU, Washington, D. C.

Menzies, M. A., W. M. Fan, and M. Zhang (1993), Palaeozoic and Cenozoic lithoprobes and the loss of >120 km of Archaean lithosphere, Sino-Korean craton, China, in *Magmatic Processes and Plate Tectonics*, *Geol. Soc. Spec. Publ.*, *76*, 71–78.

Pearson, D. G., S. B. Shirey, R. W. Carlson, F. R. Boyd, N. P. Pokhilenko, and N. Shimizu (1995), Re-Os, Sm-Nd and Rb-Sr isotope evidence for thick Archean lithospheric mantle beneath the Siberian craton modified by multi-stage metasomatism, *Geochim. Cosmochim. Acta*, *59*, 959–977.

Peng, Z. C., R. E. Zartman, E. Futa, and D. G. Chen (1986), Pb-, Sr- and Nd isotopic systematics and chemical characteristics of Cenozoic basalts, eastern China, *Chem. Geol.*, *59*, 3–33.

Peslier, A. H., D. Francis, and J. Ludden (2002), The lithospheric mantle beneath continental margin: Melting and melt-rock interactions in Canadian Cordillera xenoliths, *J. Petrol.*, *43*, 2013–2047.

Prouteau, G., B. Scaillet, M. Pichavant, and R. Maury (2001), Evidence for mantle metasomatism by hydrous silicic melts derived from subducted oceanic crust, *Nature*, *410*, 197–200.

Qiu, J. S., X. S. Xu, and Q. H. Lo (2002), Potash-rich volcanic rocks and lamprophyres in western Shandong province: ^{40}Ar-^{39}Ar dating and source tracing, *Chin. Sci. Bull.*, *47*, 91–99.

Rapp, R. P., N. Shimizu, M. D. Norman, and G. S. Applegate (1999), Reaction between slab-derived melts and peridotite in the mantle wedge: Experimental constraints at 3.8 Gpa, *Chem. Geol.*, *160*, 335–356.

Rudnick, R. L., S. Gao, W.-L. Ling, Y.-S. Liu, and W. F. McDonough (2004), Petrology and geochemistry of spinel peridotite xenoliths from Hannuoba and Qixia, North China craton, *Lithos*, *77*, 609–637.

Schiano, P., R. Clocchiatti, N. Shimizu, R. C. Maury, K. P. Jochum, and A. W. Hofmann (1995), Hydrous, silica-rich melts in the sub-arc mantle and their relationship with erupted arc lavas, *Nature*, *377*, 595–600.

Schmidt, K. H., P. Bottazzi, R. Vannucci, and K. Mengel (1999), Trace element partitioning between phlogopite, clinopyroxene and leucite lamproite melt, *Earth Planet. Sci. Lett.*, *168*, 287–299.

Smith, D., and J. C. A. Riter (1997), Genesis and evolution of low-Al orthopyroxene in spinel peridotite xenoliths, Grand Canyon field, Arizona, USA, *Contrib. Mineral. Petrol.*, *127*, 391–404.

Smith, D., J. C. A. Riter, and S. A. Mertzman (1999), Water-rock interactions, orthopyroxene growth, and Si-enrichment in the mantle: Evidence in xenoliths from the Colorado Plateau, southwestern United States, *Earth Planet. Sci. Lett.*, *167*, 347–356.

Tatsumoto, M., A. R. Basu, W. Huang, J. Wang, and G. Xie (1992), Sr, Nd, and Pb isotopes of ultramafic xenoliths in volcanic rocks of eastern China: Enriched components EMI and EMII in subcontinental lithosphere, *Earth Planet. Sci. Lett.*, *113*, 107–128.

Tsuchiya, N., S. Suzuki, J.-I. Kimura, and H. Kagami (2005), Evidence for slab melt/mantle reaction: Petrogenesis of Early Cretaceous and Eocene high-Mg andesites from the Kitakami Mountains, Japan, *Lithos*, *79*, 179–206.

Walker, R. J., R. W. Carlson, and S. B. Shirey (1989), Os, Sr, Nd and Pb isotope systematics of southern African peridotite xenoliths: Implications for the chemical evolution of subcontinental mantle, *Geochim. Cosmochim. Acta*, *53*, 1583–1595.

Wilde, S. A., X. Zhou, A. A. Nemchin, and M. Sun (2003), Mesozoic crust-mantle interaction beneath the North China Craton: A consequence of the dispersal of Gondwanaland and accretion of Asia, *Geology*, *31*, 817–820.

Wu, F. Y., R. J. Walker, X. W. Ren, D. Y. Sun, and X. H. Zhou (2003), Osmium isotopic constraints on the age of lithospheric mantle beneath northeastern China, *Chem. Geol.*, *196*, 107–129.

Xu, W. L., X. G. Ci, C. Yuan, Y. M. Huang, and W. Wang (1993), *Mesozoic Dioritic Rocks and Their Deep-Seated Rock Xenoliths in the Middle Zone of North China Craton* (in Chinese), 164 pp., Geology Press, Beijing.

Xu, W. L., D. Y. Wang, S. Gao, and J. Q. Ling (2003a), Discovery of dunite and pyroxenite xenoliths in Mesozoic diorite at Jinling, western Shandong and its significance, *Chin. Sci. Bull.*, *48*, 1599–1604.

Xu, W. L., D. Y. Wang, Q. H. Wang, and J. Q. Lin (2003b), Petrology and geochemistry of two types of mantle-derived xenoliths in Mesozoic diorite from western Shandong province (in Chinese), *Acta Petrol. Sin.*, *19*, 623–636.

Xu, W., D. Wang, Q. Wang, S. Gao, and J. Lin (2004a), Metasomatism of silica-rich melts (liquids) in dunite xenoliths from western Shandong, China: Implication for Mesozoic lithospheric mantle thinning (in Chinese), *Acta Geol. Sin.*, *78*, 72–80.

Xu, W., D. Wang, Q. Wang, F. Pei, and J. Lin (2004b), ^{40}Ar/^{39}Ar dating of hornblende and biotite in Mesozoic intrusive complex from North China block: Constraints of the time of lithosphere thinning (in Chinese), *Geochimica*, *33*, 221–231.

Xu, W., Q. Wang, D. Wang, F. Pei, and S. Gao (2004c), Processes and mechanism of Mesozoic lithospheric thinning in eastern North China Craton: Evidence from Mesozoic

igneous rocks and deep-seated xenoliths (in Chinese), *Earth Sci. Frontiers*, *11*, 309–317.

Xu, Y. G. (2001), Thermo-tectonic destruction of the Archaean lithospheric keel beneath the Sino-Korean Craton in China: Evidence, timing and mechanism, *Phys. Chem. Earth, Part A*, *26*, 747–757.

Xu, Y. G., X.-L. Huang, J.-L. Ma, Y.-B. Wang, Y. Iizuka, J.-F. Xu, Q. Wang, and X.-Y. Wu (2004), Crust-mantle interaction during the tectono-thermal reactivation of the North China Craton: Constraints from SHRIMP zircon U-Pb chronology and geo-chemistry of Mesozoic plutons from western Shandong, *Contrib. Mineral. Petrol.*, *147*, 750–767.

Yan, J., J. F. Chen, Z. Xie, and T. X. Zhou (2003), Mantle xenoliths from Late Cretaceous basalt in eastern Shandong Province: New constraint on the timing of lithospheric thinning in eastern China, *Chin. Sci. Bull.*, *48*, 2139–2144.

Yang, J. H., and X. H. Zhou (2001), Rb-Sr, Sm-Nd, and Pb isotope systematics of pyrite: Implications for the age and genesis of lode gold deposits, *Geology*, *29*, 711–714.

Yang, J. H., F. Y. Wu, and S. A. Wilde (2003), A review of the geodynamic setting of large-scale Late Mesozoic gold mineralization in the North China Craton: An association with lithospheric thinning, *Ore Geol. Rev.*, *23*, 125–152.

Yang, J.-H., S.-L. Chung, M.-G. Zhai, and X.-H. Zhou (2004), Geochemical and Sr-Nd-Pb isotopic compositions of mafic dikes from the Jiaodong Peninsula, China: Evidence for vein-plus-peridotite melting in the lithospheric mantle, *Lithos*, *73*, 145–160.

Ying, J. F. (2002), Geochemical characteristics and petrogenesis of Mesozoic carbonatites and volcanics rocks in west Shandong Province, China (in Chinese), Ph.D. thesis, Inst. of Geol. and Geophys., Chin. Acad. of Sci., Beijing.

Ying, J., X. Zhou, and H. Zhang (2004), Geochemical and isotopic investigation of the Laiwu-Zibo carbonatites from western Shandong Province, China, and implications for their petrogenesis and enriched mantle source, *Lithos*, *75*, 413–426.

Zhai, M., R. Zhu, J. Liu, Q. Meng, Q. Hou, S. Hu, W. Liu, Z. Li, H. Zhang, and H. Zhang (2004), Time range of Mesozoic tectonic regime inversion in eastern North China Block, *Sci. China, Ser. D*, *47*, 151–159.

Zhang, H. F., M. Sun, X. H. Zhou, W. M. Fan, M. G. Zhai, and J. F. Yin (2002), Mesozoic lithosphere destruction beneath the North China Craton: Evidence from major, trace element, and Sr-Nd-Pb isotope studies of Fangcheng basalts, *Contrib. Mineral. Petrol.*, *144*, 241–253.

Zhang, H. F., M. Sun, X. H. Zhou, W. M. Fan, and J. P. Zheng (2003), Secular evolution of the lithosphere beneath the eastern North China Craton: Evidence from Mesozoic basalts and high-Mg andesites, *Geochim. Cosmochim. Acta*, *67*, 4373–4387.

Zhang, H. F., M. Sun, M. F. Zhou, W. M. Fan, X. H. Zhou, and M. G. Zhai (2004), Highly heterogeneous Late Mesozoic lithospheric mantle beneath the North China Craton: Evidence from Sr-Nd-Pb isotopic systematics of mafic igneous rocks, *Geol. Mag.*, *141*, 55–62.

Zheng, C. Q., W. L. Xu, and D. Y. Wang (1999), The petrology and mineral chemistry of the deep-seated xenoliths in Mesozoic basalt in Fuxin district from western Liaoning (in Chinese), *Acta Petrol. Sin.*, *15*, 616–622.

Zhou, X., J. Yang, and L. Zhang (2002), Metallogenesis of super-large gold deposits in Jiaodong region and deep processes of subcontinental lithosphere beneath North China Craton in Mesozoic, *Sci. China, Ser. D*, *46*, suppl., 14–25.

Zou, H., A. Zindler, X. Xu, and Q. Qi (2000), Major, trace element, and Nd, Sr and Pb isotope studies of Cenozoic basalts in SE China: Mantle sources, regional variations, and tectonic significance, *Chem. Geol.*, *171*, 33–47.